Cell Reports

Article

Peroxisomal ERK mediates Akh/glucagon action and glycemic control

Graphical abstract

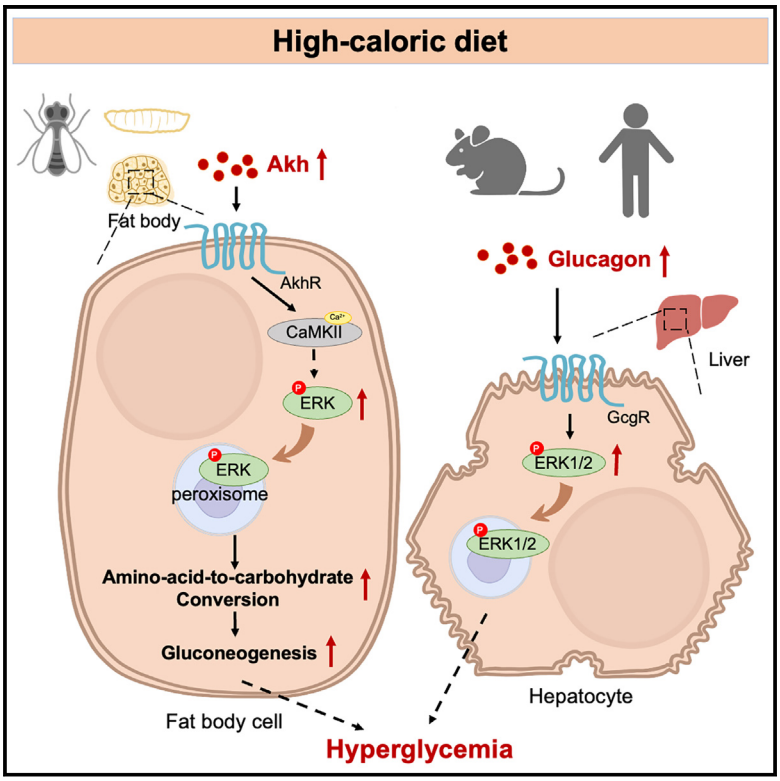

Highlights

- Akh/glucagon promotes peroxisomal ERK translocation
- Peroxisomal ERK translocation is required for diet-induced hyperglycemia
- Akh increases peroxisomal conversion of amino acids to carbohydrates via ERK
- Liver peroxisomal ERK is correlated to blood glucagon and glucose levels in obese patients

Authors

Jiaying Li, Peixuan Dang, Zhen Li, ..., Dingyu Pan, Yufeng Yuan, Wei Song

Correspondence

pandingyu@znhospital.cn (D.P.), yuanyf1971@whu.edu.cn (Y.Y.), songw@whu.edu.cn (W.S.)

In brief

The spatial regulation of Akh/glucagon signaling remains elusive. Li et al. show that Akh/glucagon promotes peroxisomal ERK translocation and peroxisome-associated gluconeogenesis, leading to hyperglycemia in *Drosophila*. They also report the correlations between liver peroxisomal ERK and blood glucagon and glucose levels in obese mice and patients.

Li et al., 2023, Cell Reports *42*, 113200
October 31, 2023
https://doi.org/10.1016/j.celrep.2023.113200

CellPress

Cell Reports

CellPress
OPEN ACCESS

Article

Peroxisomal ERK mediates Akh/glucagon action and glycemic control

Jiaying Li,[1,2,4] Peixuan Dang,[1,2,4] Zhen Li,[1,4] Tujing Zhao,[3] Daojun Cheng,[3] Dingyu Pan,[1,*] Yufeng Yuan,[1,2,*] and Wei Song[1,2,5,*]

[1]Department of Hepatobiliary and Pancreatic Surgery, Frontier Science Center for Immunology and Metabolism, Medical Research Institute, Zhongnan Hospital of Wuhan University, Wuhan University, Wuhan, Hubei 430071, China
[2]TaiKang Center for Life and Medical Sciences, Wuhan University, Wuhan, Hubei 430071, China
[3]State Key Laboratory of Silkworm Genome Biology, Southwest University, Chongqing 400715, China
[4]These authors contributed equally
[5]Lead contact
*Correspondence: pandingyu@znhospital.cn (D.P.), yuanyf1971@whu.edu.cn (Y.Y.), songw@whu.edu.cn (W.S.)
https://doi.org/10.1016/j.celrep.2023.113200

SUMMARY

The enhanced response of glucagon and its *Drosophila* homolog, adipokinetic hormone (Akh), leads to high-caloric-diet-induced hyperglycemia across species. While previous studies have characterized regulatory components transducing linear Akh signaling promoting carbohydrate production, the spatial elucidation of Akh action at the organelle level still remains largely unclear. In this study, we find that Akh phosphorylates extracellular signal-regulated kinase (ERK) and translocates it to peroxisome via calcium/calmodulin-dependent protein kinase II (CaMKII) cascade to increase carbohydrate production in the fat body, leading to hyperglycemia. The mechanisms include that ERK mediates fat body peroxisomal conversion of amino acids into carbohydrates for gluconeogenesis in response to Akh. Importantly, *Akh receptor* (*AkhR*) or *ERK* deficiency, importin-associated ERK retention from peroxisome, or peroxisome inactivation in the fat body sufficiently alleviates high-sugar-diet-induced hyperglycemia. We also observe mammalian glucagon-induced hepatic ERK peroxisomal translocation in diabetic subjects. Therefore, our results conclude that the Akh/glucagon-peroxisomal-ERK axis is a key spatial regulator of glycemic control.

INTRODUCTION

Insulin and glucagon play evolutionarily conserved roles in maintaining stable circulating carbohydrate levels in response to nutritional cues in both vertebrates and invertebrates.[1,2] The glucagon promotes the release of carbohydrates into circulation, while insulin enhances storages of carbohydrates from circulation. In addition to the well-established impairment of insulin response, enhanced response of glucagon under chronic high-caloric feeding also results in hyperglycemia, a common problem for patients with diabetes.[3,4]

Drosophila has emerged as an important model organism to study metabolic hormones and glycemic control.[5] *Drosophila* adipokinetic hormone (Akh) is equivalent to mammalian glucagon to elevate glycemic levels through glycogenolysis and gluconeogenesis,[6] two highly spatialized metabolic processes. For example, glycogen breakdown has been reported to occur in the autophagosome and lysosome to release glucose,[7,8] while conversion of amino acids into pyruvate or other metabolites in the peroxisome and TCA cycle in the mitochondria provides substrates to support gluconeogenesis.[9,10] Many metabolic enzymes that catalyze these processes have been characterized as well. Previous studies indicated that, similar to glucagon, Akh signals to its G-coupled receptor Akh receptor (AkhR) and activates Ca^{2+}/calcium/calmodulin-dependent protein kinase II (CaMKII) and cAMP/PKA/CREB cascades and their downstream regulators to control carbohydrate metabolism in the fat body.[6,11,12] However, beside the linear molecular cascades, the spatial modulation of intracellular Akh signaling at the organelle level associated with these signaling pathways is still largely unknown.

The extracellular signal-regulated kinase (ERK) cascade is a highly conserved mitogen-activated protein kinase (MAPK) pathway that modulates various biological processes, including proliferation, differentiation, and stress responses, in both vertebrates and invertebrates.[13] Recent studies have shown that ERK executes distinct and even opposing outcomes depending on the physiological stimulus. In addition to the well-known temporal regulation and binding competition, the spatial regulation of the ERK cascade has recently been shown to be essential for activation of downstream targets at certain organelles to execute specific physiological functions.[14] For instance, growth factors promote ERK translocation to nuclear and plasma membrane to induce proliferative and migratory programs, respectively.[15,16] Endosomal ERK targeting is triggered by certain G protein-coupled receptors (GPCRs; β_2-adrenergic

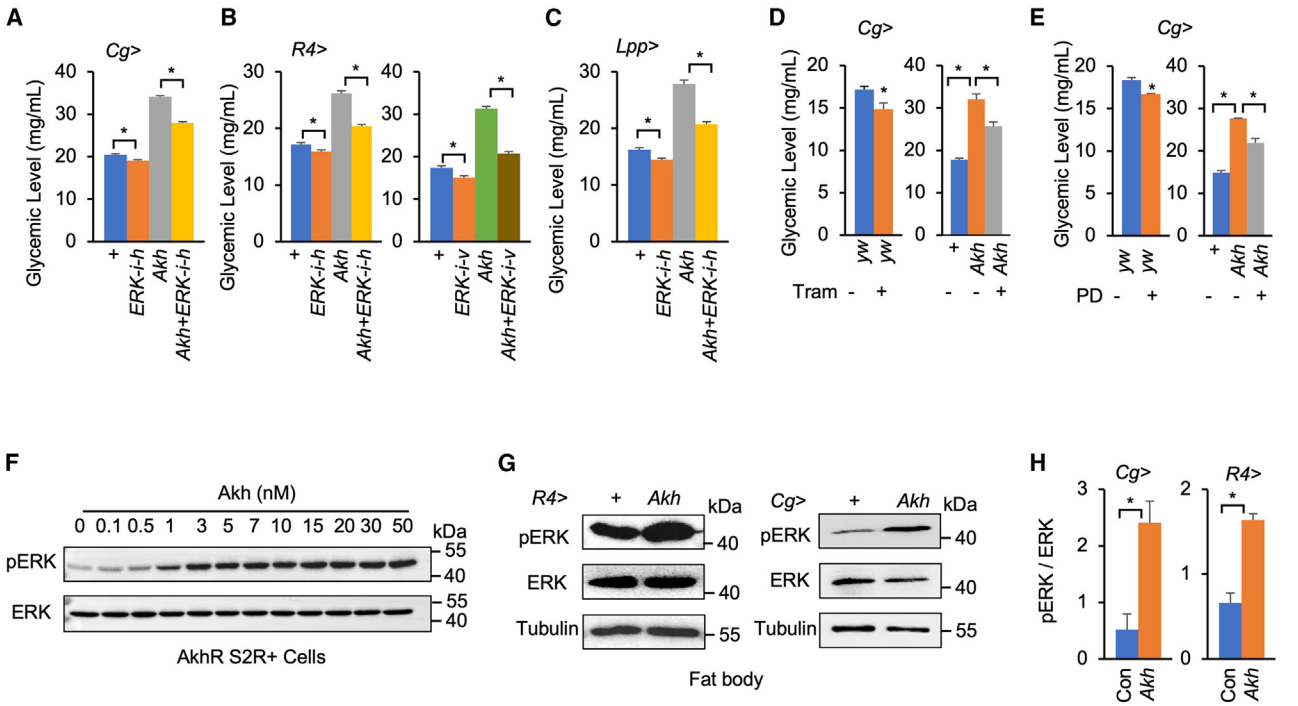

Figure 1. ERK is essential for Akh-induced hyperglycemia in *Drosophila*

(A–C) Glycemic levels, as indicated by circulating trehalose concentrations in the hemolymph, of late 3rd-instar larvae expressing Akh together with *ERK* RNAi using different fat body Gal4 drivers, including *Cg-Gal4* (A, n = 6, 8 larvae/replicate), *R4-Gal4* (B, n = 6, 8 larvae/replicate), and *Lpp-Gal4* (C, n = 8, 8 larvae/replicate).

(D and E) Glycemic levels of 3rd-instar larvae expressing Akh in the fat body under feeding of ERK inhibitors, trametinib (Tram; 50 μM, D) or PD0325901 (PD; 200 μM, E) in the fly food, throughout development (n = 3, 8 larvae/replicate).

(F and G) Immunoblots indicating phosphorylated ERK (pERK) in S2R+ cells stably overexpressing exogenous AkhR under treatment of synthetic Akh peptide for 15 min (F) and late 3rd-instar larval fat body with Akh overexpression using *R4-Gal4* (G, left) or *Cg-Gal4* (G, right).

(H) Quantification of pERK/ERK in (G) (n = 3).

Data are presented as mean ± SEM. *p < 0.05. Unpaired Student's t test and one-way ANOVA followed by post hoc test were performed to assess differences.

receptor and angiotensin II type 1 receptor) and receptor tyrosine kinases (RTKs) to regulate receptor turnover.[14,17] Mitochondrial ERK translocation is mediated by unknown stress signaling to modulate mitochondrial activity and cell apoptosis.[18] Studies in dividing cells have also indicated that the ERK cascade regulates other cellular activities via translocating to Golgi and the autophagosome, as well as cytoskeletal elements.[14,18] In addition to these proliferation-associated activities, investigating spatial ERK regulation in other compartments or organelles in non-dividing cells would be insightful for understanding the diverse effects ERK, such as maintenance of metabolic homeostasis.

In this study, we performed *in vivo* RNAi screening to identify ERK in the fat body as an important regulator of Akh-induced peroxisomal carbohydrate metabolism and hyperglycemia. Interestingly, by labeling different subcellular organelles, we found that Akh promotes ERK translocation to the peroxisome, for the first time, via Ca^{2+}/CaMKII signaling, to enhance carbohydrate production and cause hyperglycemia. Finally, we validated the conserved carbohydrate regulation by the glucagon-peroxisomal ERK axis in both obese mice and patients.

RESULTS

Fat body ERK is essential for Akh-induced hyperglycemia

We have previously performed *in vivo* RNAi screening in the fat body to identify physiological regulators of Akh response and glycemic control.[6] We found that, in addition to the hits previously identified, ERK is another strong candidate kinase potentiating Akh response (data not shown). Fat-body-specific expression of exogenous Akh has been shown to activate Akh signaling in the fat body in an autocrine manner and result in hyperglycemia,[19] making it a powerful genetic Akh-gain-of-function model for investigating intracellular regulation of Akh signaling. We first validated the results of ERK using different fat body *Gal4* lines. We consistently observed elevated glycemic levels using *R4-*, *Cg-*, and *Lpp-Gal4* to overexpress Akh in the larval fat body. Importantly, fat body *ERK* RNAi, using an RNAi line from Harvard Medical School (HMS00173, *ERK-i-h*), significantly alleviated Akh-induced hyperglycemia in larvae with Akh overexpression (Figures 1A–1C and S1A–S1C). We noticed that *ERK* knockdown in the fat body of control larvae without Akh expression only moderately decreased glycemic level (Figures 1A–1C and

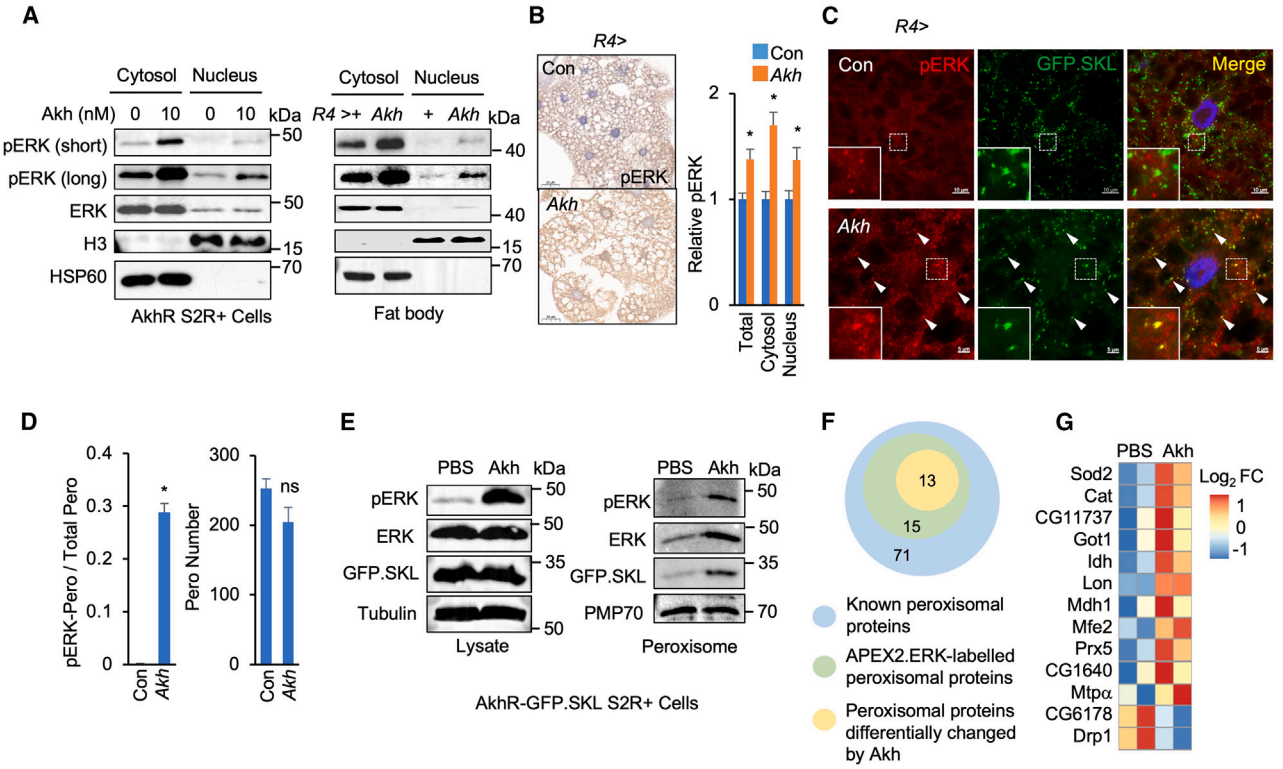

Figure 2. Akh promotes peroxisomal translocation of ERK

(A) Immunoblots indicating pERK in the cytosol and nucleus of AkhR-expressing S2R+ cells under treatment of synthetic Akh for 15 min (left) and late 3rd-instar larval fat body with Akh overexpression using *R4-Gal4* (right).

(B) Representative immunohistochemistry images indicate pERK signals in both cytoplasm and nuclear (blue) of late 3rd-instar larval fat bodies (left), and the qualification of the pERK intensity in fat body cells (right, n = 18).

(C) Confocal images indicating overlapping localization (arrowhead) of punctate pERK (red) and peroxisomes (green, GFP.SKL) in late 3rd-instar larval fat bodies with GFP.SKL together with Akh overexpression using *R4-Gal4*.

(D) Quantification of ratio of pERK-localized punctate peroxisomes (pERK-Peros) to total punctate peroxisomes (total Peros) (left) and numbers of total Peros per fat body cell (right) (n = 8).

(E) Immunoblots indicating pERK in the lysate (left) and isolated peroxisomes (right) from AkhR-GFP.SKL-expressing S2R+ cells under treatment of 10 nM synthetic Akh for 15 min.

(F and G) APEX2-labeled peroxisomal proteins (F) and the ones that were significantly changed (F and G, heatmap) in S2R+ cells stably expressing AkhR and FLAG.APEX2.ERK under treatment of 10 nM synthetic Akh for 30 min.

Data are presented as mean ± SEM. *p < 0.05. Unpaired Student's t test and one-way ANOVA followed by post hoc test were performed to assess differences.

S1D–S1I). These results indicated that fat body ERK is essential for Akh-induced hyperglycemia. To exclude the possibilities of off-target RNAi, we also included another independent *ERK* RNAi line from VDRC (109108, *ERK-i-v*) or fed larvae small-molecular inhibitors of ERK cascade, Trametinib (Tram) and PD0325901 (PD), and observed similar results that fat body ERK deficiency or inactivation alleviated Akh-induced hyperglycemia (Figures 1B–1E).

We also examined whether Akh autonomously activates ERK. We treated S2R+ cells that stably express exogenous AkhR with synthetic Akh and, notably, found a robust dose-dependent increase of ERK phosphorylation (pERK) (Figure 1F). We next examined pERK in the fat body and consistently observed that fat body pERK was increased by Akh ectopic overexpression (Figures 1G and 1H). Taken together, these results demonstrate that Akh increases the glycemic level through ERK activation in the fat body.

Akh increases peroxisomal ERK translocation in the fat body

The function of ERK is not only dependent on its phosphorylation but also on its translocation to different organelles. To investigate how Akh regulates intracellular ERK translocation, we treated S2R+ cells that stably express AkhR with synthetic Akh for 15 min. As shown by immunoblot, the treatment increased pERK levels in both the nucleus and cytosol (Figure 2A, left). Similar results were observed in the larval fat body with ectopic Akh overexpression (Figure 2A, right). Immunohistochemistry (IHC) further confirmed the elevation in pERK levels in both the nucleus and cytosol of larval fat body under Akh stimulation (Figure 2B). We next used reporters to label different organelles and examined t which organelle(s) Akh translocates ERK. Strikingly, confocal images indicated that Akh potently increased pERK translocation to peroxisomes that were labeled by GFP.SKL, a GFP with a C-terminal peroxisomal localization signal,[20] without

affecting peroxisome masses in the larval fat body (Figures 2C and 2D). Akh also slightly increased pERK translocation to the mitochondria, endoplasmic reticulum (ER), and Golgi apparatus (Figures S2A and S2B). To avoid non-specific staining, we performed immunostaining using secondary antibody only and did not observe any obvious signals (Figure S2C).

Next, we generated S2R+ cells that stably express AkhR and GFP.SKL to confirm the effects of Akh on intracellular pERK translocation. As expected, we found that the amounts of ERK and pERK, as well as GFP.SKL in isolated peroxisomes, which were labeled by peroxisomal membrane protein PMP70,[21] were increased by Akh (Figures 2E and S3A). Finally, we performed proximity labeling of proteins nearby ERK by expressing a fused protein with an engineered peroxidase APEX2 conjugated to the N terminus of ERK (FLAG.APEX2.ERK)[22,23] together with AkhR in S2R+ cells (Figure S3B). Streptavidin-HRP blotting assays showed robust APEX2-mediated biotinylation of intracellular proteins after treatment with biotin-phenol and H_2O_2, as compared to endogenous protein biotinylation at basal condition without H_2O_2 treatment (Figure S3C). We next enriched biotinylated proteins in the lysates of cells after Akh treatment, which activated fused FLAG.APEX2.ERK and translocated it to peroxisomes (Figures S3D and S3E), using streptavidin beads and performed mass spectrometry (MS)-based proteomic analysis. Interestingly, we found that Akh significantly increased the biotinylation of 11 proteins, while it decreased the biotinylation of 2 proteins, among 99 previously established peroxisomal proteins (Figures 2F and 2G; Table S1). This suggested a promoted interaction between ERK and these peroxisomal proteins, which were putatively involved in amino acid-to-carbohydrate conversion (Got1, Idh, Mdh1, CG1640), lipid metabolism (CG11737, Mfe2, Mtpα, CG6178) and stress responses (Sod2, Cat, Lon, Prx5, Drp1). Note that, consistent with confocal images of ERK translocation (Figures S2A and S2B), the MS results also indicated an increase in the interaction between ERK and mitochondrial, ER, or Golgi proteins (Figure S4C).

We wondered whether Akh promotes peroxisomal ERK translocation under physiological conditions. To investigate this, we measured ERK translocation in the fat bodies that were subjected to a short-term starvation, which has been shown to increase Akh release and fat body response to Akh in larvae.[6,24] As expected, we found that starvation increased translocation of pERK to peroxisomes, which were labeled by PMP70, in the control fat body (Figures S4D and S4E), albeit to a lesser extent than the effects of ectopic Akh expression. We then measured ERK translocation in Akh-null mutants (Akh^{A}) and found that peroxisomal ERK translocation in the fat body in response to starvation was remarkably diminished without affecting the peroxisomal masses (Figures S4D and S4E), suggesting that Akh is required for peroxisomal ERK translocation under starvation.

Because of counter-regulation of glycemic homeostasis between Akh and insulin, we wondered whether impairing insulin signaling would also increase ERK peroxisomal translocation in a manner similar to increased Akh signaling. We knocked down *insulin receptor* (*InR*) expression in the fat body but did not observe any changes in peroxisomal pERK translocation as indicated by GFP.SKL (Figures S5A and S5B), even though the glycemic level was remarkably increased due to deficiency of insulin action (Figure S5C). In contrast, when we increased insulin signaling in the fat body by overexpressing an active InR (InR^{AC}), we failed to observe peroxisomal pERK translocation as well (Figures S5A and B). We also examined the glycemic control between fat body ERK and insulin signaling. We found that *ERK* knockdown in larval fat body potently alleviated the hyperglycemia caused by *InR* deficiency (Figure S5C, left), indicating a genetic interaction between ERK and insulin signaling. Nevertheless, we also observed that fat body *ERK* knockdown plus InR^{AC} overexpression caused a further decrease in glycemic level as compared to either *ERK* knockdown or InR^{AC} overexpression alone (Figure S5C, right). This suggested that ERK also executes an insulin-independent effect on glycemic control. Taken together, our results demonstrate that Akh, but not insulin, robustly increases peroxisomal ERK translocation.

Akh-ERK axis increases peroxisomal conversion of carbohydrate

We next investigated whether peroxisomal ERK translocation contributes to hyperglycemic action of Akh. Peroxisomes are key organelles that mediate glycemic control by converting circulating amino acids and fatty acids into the substrates for gluconeogenesis.[9] We therefore examined the changes in circulating metabolites in the larvae with Akh gain of function. Interestingly, the enrichment analysis of differentially regulated metabolites indicated that those involved in glycolysis, gluconeogenesis, and metabolism of amino acids, as well as purine metabolism and others, were highly enriched (Figure 3A; Table S2). For example, we found that the major gluconeogenic amino acids such as alanine, phenylalanine, arginine, and aspartate in the hemolymph were significantly decreased by Akh (Figures 3B and 3C), suggesting the consumption of them. Meanwhile, the substrates for gluconeogenesis including citrate, succinate, phosphoenolpyruvate, and glucose, as well as trehalose 6-P and trehalose, were significantly increased in the hemolymph (Figures 3B and 3C), suggesting an increase in their production. We further analyzed the circulating metabolites in the hemolymph of larvae with Akh gain of function plus fat body *ERK* knockdown. Strikingly, an Akh-associated decrease in circulating gluconeogenic amino acids and an increase in gluconeogenic substrates were potently alleviated by *ERK* knockdown (Figures 3B and 3C). These results reveal that Akh promotes peroxisomal conversion of amino acids to carbohydrates via ERK signaling.

To investigate whether Akh-associated peroxisomal carbohydrate metabolism is dependent on ERK, we simultaneously knocked down the expression of peroxisomal regulators to impair peroxisomal functions and *ERK* in the fat body. Many peroxin (Pex) family members play evolutionarily conserved roles for peroxisomal assembly and function maintenance, such as Pex7 for import, Pex13/14 for docking, and Pex1 for recycling of peroxisomal matrix proteins.[25,26] Knocking down the expression of these proteins using independent RNAi in the fat body consistently decreased the peroxisomal masses, as indicated by GFP.SKL, and potently abolished Akh-induced hyperglycemia (Figures 3D, 3E, and S6). Notably, knockdown of *ERK* in addition to *Pex*(s) in the larval fat body failed to further reduce glycemic

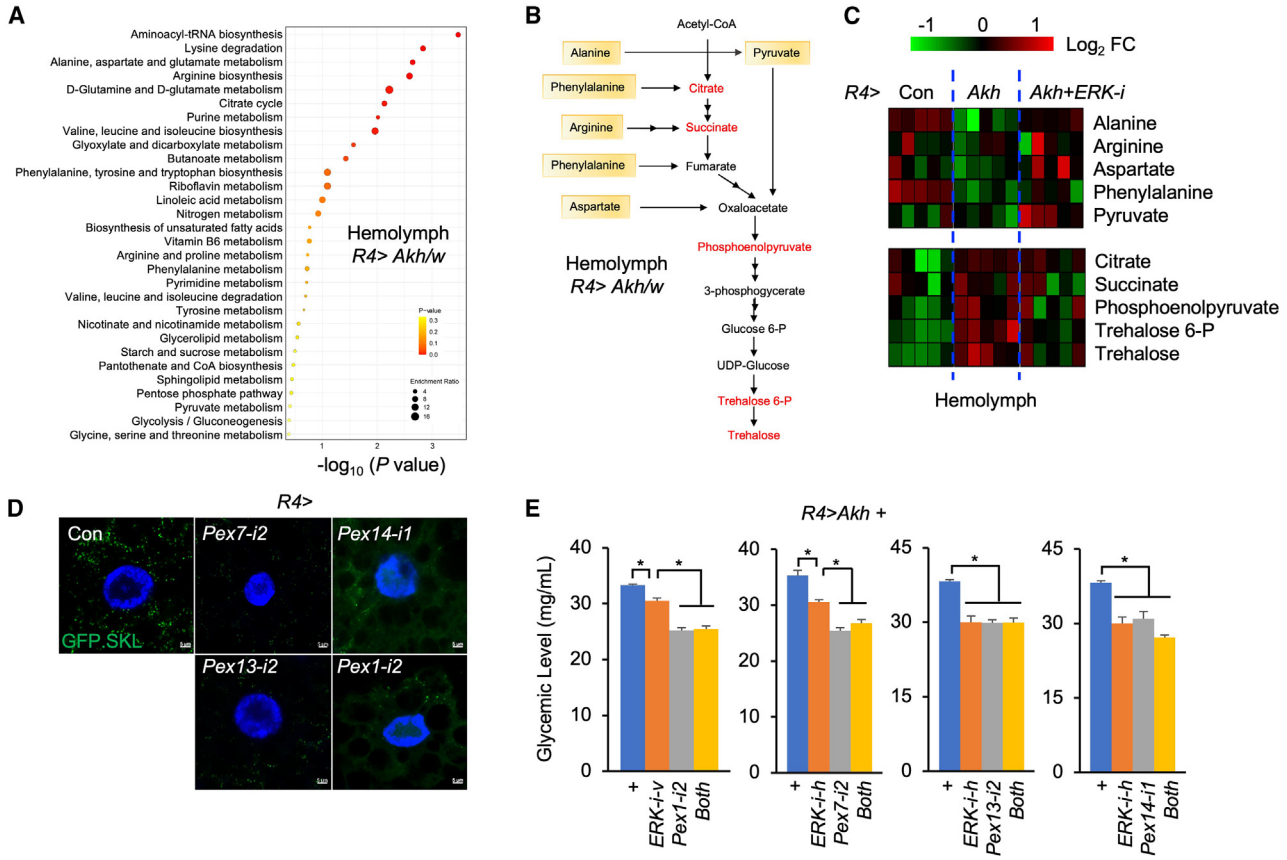

Figure 3. ERK-associated peroxisomal activity contributes to Akh action

(A) Enrichment results of circulating metabolites that were differentially changed in hemolymph of late 3rd-instar larvae with Akh overexpression in the fat body using *R4-Gal4*.

(B) The metabolites involved in conversion of glucogenic amino acids into carbohydrates from (A).

(C) Heatmap indicating relative levels of metabolites involved in conversion of glucogenic amino acids to carbohydrates in hemolymph of indicated late 3rd-instar larvae.

(D) Confocal images of punctate peroxisomes in indicated late 3rd-instar larval fat body.

(E) Glycemic levels of indicated 3rd-instar larvae with Akh overexpression plus RNAi in the fat body (n > 5, 5 larvae/replicate).

Data are presented as mean ± SEM. *p < 0.05. Unpaired Student's t test and one-way ANOVA followed by post hoc test were performed to assess differences.

levels as compared to each one of them (Figures 3D, 3E, and S6), indicating that ERK and peroxisomal function interact genetically in Akh-associated carbohydrate metabolism.

Peroxisomal ERK is required for high-caloric-diet-induced hyperglycemia

Previous studies have uncovered that chronic high-caloric diet leads to hyperglycemia by enhancing Akh signaling in the fat body.[3,6] We hypothesized that the Akh-ERK axis and peroxisomal activity in the fat body might play a role in this process. To address this hypothesis, we fed larvae a high-sugar diet (HS) to increase Akh signaling and glycemic level and meanwhile perturbed the Akh-ERK axis by knocking down the expression of *AkhR* or *ERK*. Consistent with Akh gain of function, chronic HS increased both phosphorylation and peroxisomal translocation of ERK in the fat body (Figures 4A and 4B). Fat body knockdown of *AkhR* to block Akh signaling significantly decreased both pERK and peroxisomal translocation under a HS (Figures 4A and 4B). We also found that fat body *AkhR* deficiency,[6] *ERK* knockdown, or Tram feeding to suppress ERK activity all consistently alleviated HS-induced hyperglycemia (Figures 4C–4E).

To further investigate the role of peroxisomal ERK in glycemic control, we expressed *moleskin* (*msk*), a gene encoding an importin that imports ERK from the cytoplasm into the nucleus.[27] We observed that *msk* overexpression dramatically disrupted peroxisomal ERK translocation without affecting pERK in the fat body and, strikingly, mitigated HS-induced hyperglycemia (Figures 4A–4F). Note that either HS or genetic perturbation of Akh-ERK axis did not affect the peroxisomal masses (Figure 4B), suggesting that peroxisomal function, but not mass, is important for glycemic control. We further confirmed this by knocking down key Pex(s) in the larval fat body, which also led to a decrease in HS-induced hyperglycemia (Figure 4G). Altogether, these results demonstrate that the Akh-ERK axis and peroxisomal regulation are essential for development of hyperglycemia associated with energy overload.

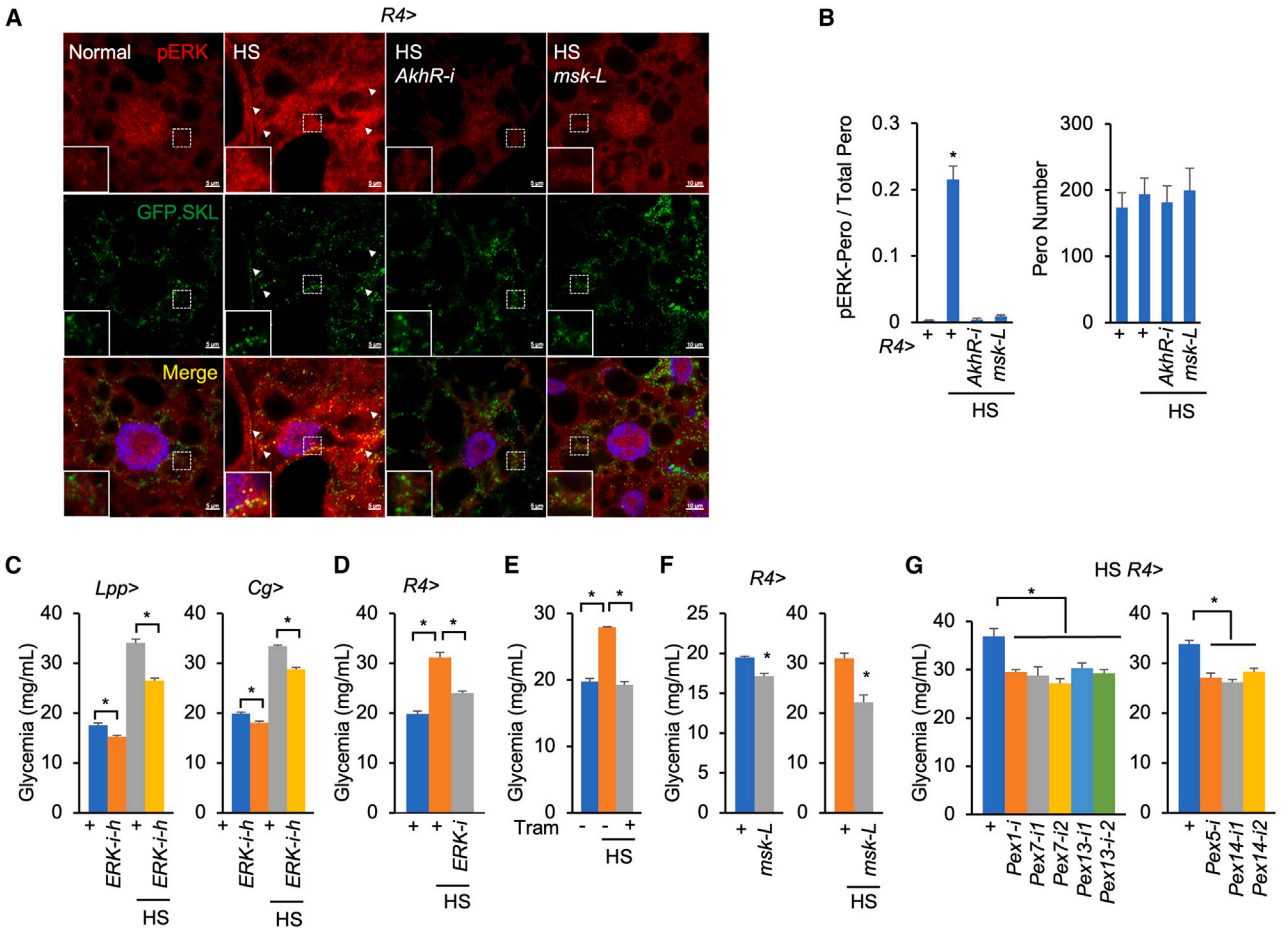

Figure 4. Peroxisomal ERK is required for HSD-associated hyperglycemia

(A) Confocal images indicating overlapping localization (arrowhead) of punctate pERK (red) and peroxisomes (green, GFP.SKL) in fat bodies of late 3rd-instar larvae with GFP.SKL expression together with genetic manipulation using *R4-Gal4* under high-sugar feeding throughout development.

(B) Quantification of ratio of pERK-Peros to total Peros (left) and numbers of total Peros per fat body cell (right) (n = 6).

(C–G) Glycemic levels of indicated 3rd-instar larvae with RNAi or gene expression in the fat body using *Lpp-Gal4* (C, left), *Cg-Gal4* (C, right), and *R4-Gal4* (D, F, and G) under chronic high-sugar feeding or inhibitor feeding throughout development (C, n = 8, 8 larvae/replicate, normal; 10 larvae/replicate, high-sugar diet [HS]; D and E, n = 3; normal, 8 larvae/replicate; HS, 10 larvae/replicate; F, n ≥ 3; normal, 8 larvae/replicate; HS, 10 larvae/replicate; G, n = 6, 10 larvae/replicate; Tram, 50 μM in the fly food).

Data are presented as mean ± SEM. *p < 0.05. Unpaired Student's t test and one-way ANOVA followed by post hoc test were performed to assess differences.

Akh increases peroxisomal ERK translocation via CaMKII signaling

We next investigated the molecular mechanism by which Akh increases peroxisomal ERK translocation. Many groups have revealed that Akh activates AkhR and its downstream cAMP/PKA and Ca^{2+}/CaMKII signaling pathways,[6,11,12] raising a hypothesis that cAMP/PKA or Ca^{2+}/CaMKII signaling might promote peroxisomal ERK translocation. To address this, we first autonomously activated cAMP/PKA signaling in the fat body by overexpressing *rutabaga* (rut), which encodes an adenylyl cyclase to synthesize cAMP,[28] and PKA catalytic subunit Pka-C1.[29] However, neither of these interventions promoted peroxisomal ERK translocation (Figures 5A and 5C). We next activated cytoplasm Ca^{2+} signaling by knocking down the expression of *SERCA*, an ER Ca^{2+} pump that increases Ca^{2+} retention into the ER,[30] or by overexpressing TrpA1, a temperature-sensitive ion channel that triggers intracellular Ca^{2+} influx.[31] Interestingly, fat body TrpA1 overexpression remarkably increased peroxisomal ERK translocation, even though *SERCA* knockdown was not sufficient to do so (Figures 5A and 5C). To examine whether Ca^{2+} signaling is required for Akh-induced peroxisomal ERK translocation, we further performed genetic blockade in the context of Akh gain of function. Impressively, we found that knockdown of either *Itpr*, an ER Ca^{2+} channel that releases Ca^{2+} into the cytoplasm,[32] or *CaMKII* potently diminished Akh-induced peroxisomal ERK translocation (Figures 5B and 5D). These results uncover that Akh promotes peroxisomal ERK translocation in a CaMKII-dependent manner.

Because ERK protein lacks peroxisomal localization signals, we hypothesize that certain ERK-binding partners downstream

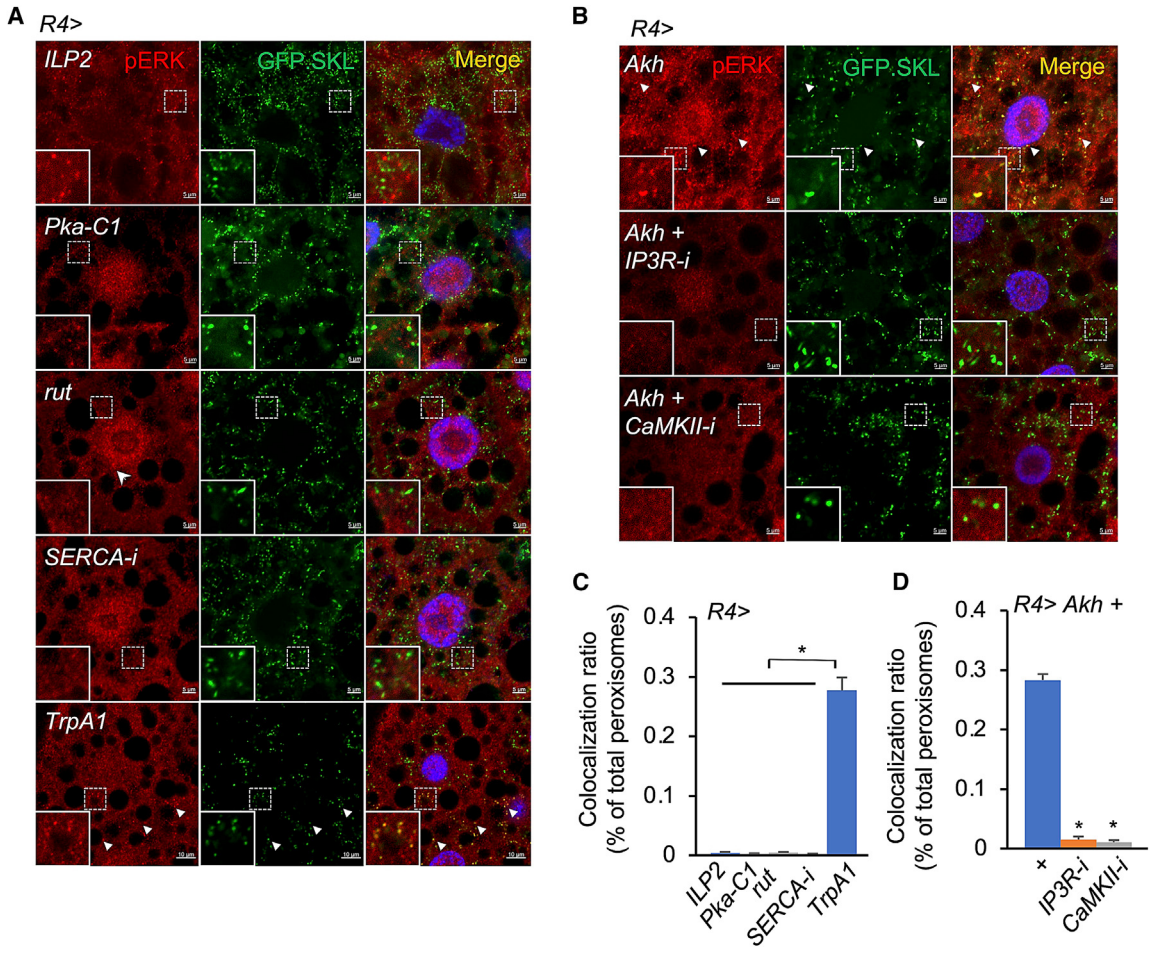

Figure 5. Akh enhances ERK peroxisomal localization via Ca^{2+} signaling

(A and B) Confocal images indicating overlapping localization (arrowhead) of punctate pERK (red) and peroxisomes (green, GFP.SKL) in fat bodies of indicated late 3rd-instar larvae with GFP.SKL expression plus genetic manipulation without (A) or with (B) Akh overexpression using *R4-Gal4*.

(C and D) Quantification of ratio of pERK-Peros to total Peros per fat body cell (n = 6).

Data are presented as mean ± SEM. *p < 0.05. Unpaired Student's t test and one-way ANOVA followed by post hoc test were performed to assess differences.

of Ca^{2+}/CaMKII signaling facilitate ERK peroxisomal translocation. We therefore searched for ERK-binding candidates from our APEX2.ERK MS dataset with three criteria: (1) with consensus sequence R-X-X-S/T for CaMKII phosphorylation[33]; (2) with Akh-increased ERK binding or APEX2.ERK labeling; and 3) with type I peroxisomal targeting signal(s) (PTS1): S/A-K/R-L/M.[34] We eventually identified two candidates (Figure S7A): Mfe2 and Mtpα. However, both of them have been characterized to localize to peroxisomes under basal conditions.[35,36] Although there is no evidence to support PTS2-mediated peroxisome protein import in *Drosophila*,[35] we hypothesized that these proteins may be imported into peroxisomes in a non-canonical manner meeting criteria 1 and 2. We performed a small-scale RNAi screening in the fat body with Akh gain of function and found that fat body knockdown of ubiquitin hydrolase *faf*, at least, significantly decreased peroxisomal ERK translocation and glycemic levels associated with Akh (Figures S7D and G). Note that Faf exhibits multiple CaMKII phosphorylation sites, an increase in Akh-induced ERK interaction, and moderate expression in the fat body[6] (Figures S7B and S7D). Taken together, our results demonstrate that Akh promotes peroxisomal ERK translocation through CaMKII signaling.

Peroxisomal ERK is associated with mammalian glucagon response and hyperglycemia

Glucagon, a well-established mammalian insulin counter-regulatory hormone that is functionally equivalent to fly Akh, modulates glycemic homeostasis partially through hepatic peroxisomal conversion of amino acids to carbohydrate.[37,38] We wondered whether the peroxisomal ERK regulation we found in *Drosophila* also contributes to mammalian glucagon action in the liver. We first treated cultured primary mouse hepatocytes with different doses of glucagon and found that ERK1/2 could be rapidly activated by glucagon at low dosages (Figure 6A). We also found that glucagon robustly increased peroxisomal ERK translocation, as indicated by co-localization of punctate pERK and a peroxisomal protein, PMP70, after treatment for 30 min (Figures 6B and 6C). Further, Tram-associated

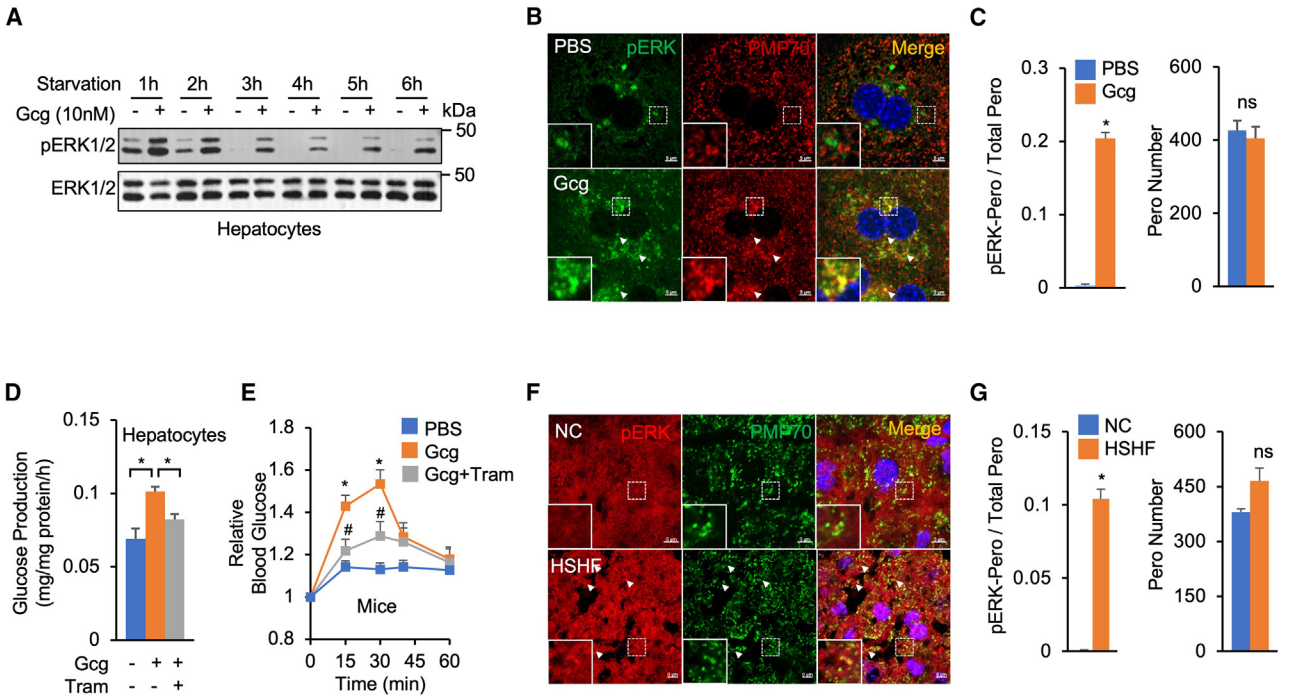

Figure 6. Glucagon promotes hepatic peroxisomal ERK localization

(A) Immunoblots indicating pERK1/2 in primary cultured hepatocytes were starved for different time points prior for treatment of 10 nM glucagon (Gcg) for 5 min.

(B) Confocal images indicating overlapping localization (arrowhead) of punctate pERK (green, anti-pERK) and peroxisomes (red, anti-PMP70) in primary cultured hepatocytes under treatment of 100 nM glucagon for 30 min.

(C) Quantification of ratio of pERK-Peros to total Peros (left) and numbers of total Peros (right) (n = 4).

(D) Glucose production in primary hepatocytes under treatment of 100 nM glucagon for 4 h together with 100 nM Tram (n > 7).

(E) Blood glucose concentrations in 8-week-old mice that were intraperitoneally (i.p.) injected 3 mg/kg/day with Tram for 5 days prior to i.p. injection of 100 μg/kg glucagon for glucagon stimulation test (n > 8).

(F) Confocal images indicating overlapping localization (arrowhead) of punctate pERK (red, anti-pERK) and peroxisomes (green, anti-PMP70) in liver of 18- to 20-week-old male mice that received a high-fat, high-sugar diet for 12 weeks.

(G) Quantification of ratio of pERK-Peros to total Peros (left) and numbers of total Peros (right) (n = 5). *p < 0.05. Gcg vs. PBS group; #p < 0.05, Gcg+Tram vs. Gcg group. Data are presented as mean ± SEM. Unpaired Student's t test and one-way ANOVA followed by post hoc test were performed to assess differences.

ERK inactivation significantly abolished glucagon-induced glucose production in both culture hepatocytes and mice (Figures 6D and 6E), suggesting that peroxisomal ERK enhances hepatic glucagon response with respect to glucose production. Given that blockade of either ERK signaling or hepatic glucagon response sufficiently alleviates high-caloric-diet-induced hyperglycemia,[39–41] we hypothesized that peroxisomal ERK is also involved in diet-induced hyperglycemia. We examined the intracellular pERK localization in the liver of mice under high-sugar, high-fat feeding (HSHF) and, interestingly, found a remarkable increase in peroxisomal pERK translocation (Figures 6F and 6G), an event associated with hyperglycemia and enhanced hepatic glucagon response,[42,43] as compared with normal chow feeding (NC). These results indicate that peroxisomal ERK and glucagon responses are involved in high-caloric-diet-induced hyperglycemia.

Finally, we investigated whether peroxisomal ERK translocation is associated with human diabetes. We examined the ERK localization in the hepatocytes of liver from 33 obese patients, 19 of whom were diagnosed with hyperglycemia or diabetes, while 14 were diagnosed with euglycemia (Table S3). We compared the hepatic pERK localization of diabetic and non-diabetic obese patients. Interestingly, the peroxisomal ERK translocation was significantly increased in the hepatocytes of patients with diabetes as compared with non-diabetic ones (Figures 7A and 7B). The overall hepatic pERK levels in patients with diabetes were also higher, probably due to other inflammatory signals (Figure 7A). We further observed a significant positive correlation between the ratios of hepatic peroxisomal ERK and blood glucose levels in the patients (Figure 7C). Because peroxisomal ERK translocation is controlled by glucagon, we also examined the blood glucagon levels and, as expected, found a positive correlation between hepatic peroxisomal ERK translocation and blood glucagon levels in the patients (Figure 7D). Taken together, these results indicate that peroxisomal ERK is highly associated with glucagon response and hyperglycemia in both obese mice and humans.

DISCUSSION

Since the spatial regulation of Akh/glucagon response and glycemic control at the organelle level in unknown, we combined

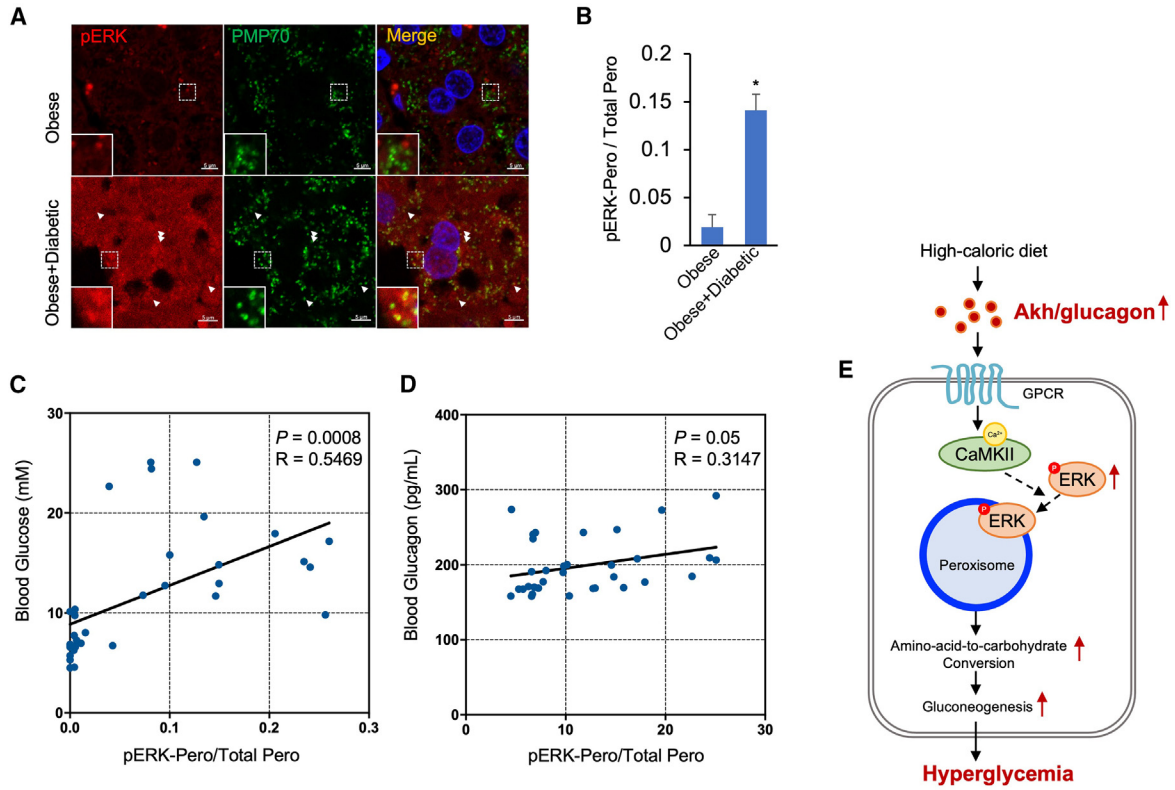

Figure 7. Hepatic ERK peroxisomal translocation in patients with diabetes

(A) Confocal images indicating overlapping localization (arrowhead) of punctate pERK (red, anti-pERK) and peroxisomes (green, anti-PMP70) in liver of obese patients diagnosed as diabetic.

(B) Quantification of ratio of pERK-Peros to total Peros (n > 15).

(C and D) Correlation between pERK-Pero ratio and blood glucose levels (C) or glucagon levels (D) in all obese patients. Date were analyzed by Prism7.0 software using Pearson correlation analysis.

(E) Schematic model of Akh/glucagon promoting peroxisomal ERK translocation in both flies and mice.

Data are presented as mean ± SEM. *p < 0.05. Unpaired Student's t test and one-way ANOVA followed by post hoc test were performed to assess differences.

studies in fly and mammals to demonstrate the essential roles of peroxisomal ERK translocation and peroxisomal carbohydrate metabolism in Akh/glucagon signaling and diet-induced hyperglycemia across species. We further revealed that the Ca^{2+}/CaMKII cascade, but not the cAMP/PKA pathway, contributes to ERK translocation onto peroxisome.

Akh has been shown to elevate glycemic levels through glycogenolysis and gluconeogenesis, two metabolic processes that occur in specialized subcellular compartments. For instance, glycogen is broken down in the autophagosome and lysosome to release glucose.[7,8] Circulating amino acids are delivered into the peroxisome to convert into pyruvate or other metabolites that can be used for gluconeogenesis.[9] The TCA cycle in mitochondria also provides substrates for glucose synthesis. In this study, we found that Akh predominantly translocases pERK to the peroxisomes to impact carbohydrate metabolism regarding glycemic control. It is the first evidence for ERK peroxisomal translocation, as opposed to the well-known subcellular localization of ERK. Our results thus provide novel insights into spatial ERK regulation of carbohydrate metabolism and Akh-induced hyperglycemia.

Even though we failed to find autophagosomal or lysosomal ERK translocation by Akh, we did observe that a small portion of pERK translocates to mitochondria (Figures S2, S3, and S4C). Consistent with the notion that conversion of oxaloacetate into phosphoenolpyruvate (PEP) in mitochondria supports gluconeogenesis, our results revealed that Akh increased PEP release into circulating in an ERK-dependent manner (Figures 3B and 3C), suggesting that mitochondrial ERK translocation might also participate in Akh-associated carbohydrate metabolism. It would be very insightful to investigate how ERK translocation to individual organelles, such as peroxisome, mitochondria, ER, and Golgi, collectively modulates metabolic homeostasis in future study.

How ERK enhances peroxisome activity with respect to carbohydrate synthesis is an interesting question to address. The most convincing evidence in this study included that our APEX2 assays in S2R+ cells revealed ERK interaction with a few peroxisomal proteins, including CG1640 (GPT1/2), Got1, and Mdh1, which catalyze the conversion of amino acids to gluconeogenic substrates, under Akh stimulation (Figures 2F and 2G). It is possible that ERK directly activates these metabolic enzymes in peroxisome to promote gluconeogenesis. Second, we

observed that Akh stimulation increases peroxisomal translocation of both pERK and GFP.SKL in S2R+ cells (Figure 2E, right), indicating a correlation between ERK activation and import of peroxisomal proteins. A recent study interestingly uncovered that mammalian ERK1/2 phosphorylates Pex14, which regulates overall import of peroxisomal proteins,[44] consistently suggesting that ERK might control general peroxisomal protein import to affect gluconeogenesis. Finally, Akh enhances ERK interaction with a few anti-oxidant proteins such as Sod2, Cat, Lon, and Prx5 (Figures 2F and 2G). Because redox balance is critical for peroxisomal integrity and functions, it is also possible that ERK impacts these anti-oxidant regulators to maintain peroxisome activity.

To exploit the mechanisms how Akh promotes peroxisomal ERK translocation, we examined the major regulators of Akh signaling, including the cAMP/PKA and Ca^{2+}/CaMKII cascades. Interestingly, only the Ca^{2+}/CaMKII cascade robustly enhances peroxisomal ERK translocation. Because no PTS was found in ERK protein, we speculated that certain binding proteins facilitate ERK translocation downstream CaMKII signaling. However, the only two candidates that met all three criteria—(1) had a CaMKII phosphorylation site, (2) had PTS1 at the C terminus, and (3) increased binding to ERK by Akh—from our MS dataset were Mfe2 and Mtpa, two established proteins residing in peroxisome in the absence of Akh treatment. This suggested the involvement of non-canonical peroxisomal import. After performing RNAi screening of candidates with both CaMKII phosphorylation site(s) and increased binding to ERK by Akh, we so far found that knockdown of at least *Faf* significantly diminished Akh-induced peroxisomal ERK translocation and hyperglycemia. Future validation using more comprehensive tools would be helpful to elucidate detailed mechanisms.

Systemic pharmaceutical inhibition of ERK has been established to improve high-caloric-diet-induced hyperglycemia in mammals. Despite the evidence that ERK modulates Cdk5/PPARγ signaling and lipolytic programs in the adipose tissues to cause insulin resistance and impair glucose uptake,[41,45] the molecular mechanisms of how ERK perturbs hepatic glucose production are not well understood. Previous studies have revealed that activation of hepatic ERK signaling causes hyperglycemia and suggested that this could be caused by cytosolic FOXO1 retention and impaired lipid oxidation, as well as feedback regulation of PKA activity.[46–48] However, the direct evidence of how ERK perturbs hepatic glucose production, especially in a spatial fashion, is still missing. In this study, we uncovered that mouse glucagon enhances peroxisomal ERK translocation in the liver and promotes hepatic glucose production in an ERK-dependent manner. The clinical observations in obese patients further indicated the positive correlation between hepatic peroxisomal ERK translocation, circulating glucagon levels, and hyperglycemia. These results collectively demonstrate the conserved roles of the Akh/glucagon-peroxisomal ERK axis in glycemic control from *Drosophila* to human and provide novel therapeutic opportunities targeting peroxisomal ERK in diabetes treatment.

Limitations of study

While we noticed that ERK knockdown in the larval fat body suppresses Akh-induced conversion of amino acids into carbohydrates and reduces hyperglycemia, it remains uncertain whether this regulation relies on peroxisomal ERK translocation. Conversely, the associations observed in obese mice and patients imply that hepatic peroxisomal ERK translocation could contribute to hyperglycemia. Nevertheless, additional validation is required to substantiate this hypothesis.

STAR★METHODS

Detailed methods are provided in the online version of this paper and include the following:

- KEY RESOURCES TABLE
- RESOURCE AVAILABILITY
  - Lead contact
  - Materials availability
  - Data and code availability
- EXPERIMENTAL MODEL AND STUDY PARTICIPANTS DETAILS
  - Fly strains and rearing
  - Mouse models
  - Human samples
  - Primary hepatocyte isolation and culture
- METHOD DETAILS
  - Carbohydrate measurements in 3rd instar larvae
  - Generation of stable AkhR- and Apex2.ERK-expressing S2R + cells
  - APEX2 reaction and biotinylated protein capture
  - Proteomics and data analysis
  - Metabolomics and data analysis
  - Hepatocyte glucose production
  - Organelle isolation and Western blotting
  - Generation of rabbit polyclonal anti-PMP70 antibodies
  - Immunostaining and immunohistochemistry
- QUALIFICATION AND STATISTICAL ANALYSIS

SUPPLEMENTAL INFORMATION

Supplemental information can be found online at https://doi.org/10.1016/j.celrep.2023.113200.

ACKNOWLEDGMENTS

We thank the BDSC, VDRC, NIG, and TsingHua Fly Center for providing fly stocks; the Core Facility of Drosophila Resource and Technology, Center for Excellence in Molecular Cell Science, Chinese Academy of Sciences, for providing fly stocks; and Drs. Yong Liu (Wuhan University), Shangyu Hong (Fudan University), and Baoliang Song (Wuhan University) for insightful comments and technical support. Work in the Song lab was supported by the National Natural Science Foundation of China (91957118, 31800999, and 31971079), the Ministry of Science and Technology of China (National Key R&D Program of China 2021YFC2700704), and the Fundamental Research Funds for the Central Universities (2042022dx0003).

AUTHOR CONTRIBUTIONS

J.L. and P.D. performed fly and mouse experiments. J.L., P.D., and Z.L. handled patient samples. T.Z. and D.C. performed ERK RNAi in the fat body. D.P., Y.Y., and W.S. analyzed results. W.S. wrote manuscript.

DECLARATION OF INTERESTS

The authors declare no competing interests.

Received: April 5, 2023
Revised: June 18, 2023
Accepted: September 15, 2023

REFERENCES

1. Haselton, A.T., and Fridell, Y.W.C. (2010). Adult Drosophila melanogaster as a model for the study of glucose homeostasis. Aging (Albany NY) *2*, 523–526.
2. Unger, R.H. (1971). Glucagon and the insulin: glucagon ratio in diabetes and other catabolic illnesses. Diabetes *20*, 834–838.
3. Musselman, L.P., Fink, J.L., Narzinski, K., Ramachandran, P.V., Hathiramani, S.S., Cagan, R.L., and Baranski, T.J. (2011). A high-sugar diet produces obesity and insulin resistance in wild-type Drosophila. Dis. Model. Mech. *4*, 842–849. https://doi.org/10.1242/dmm.007948.
4. Buettner, R., Schölmerich, J., and Bollheimer, L.C. (2007). High-fat diets: modeling the metabolic disorders of human obesity in rodents. Obesity *15*, 798–808. https://doi.org/10.1038/oby.2007.608.
5. Chatterjee, N., and Perrimon, N. (2021). What fuels the fly: Energy metabolism in Drosophila and its application to the study of obesity and diabetes. Sci. Adv. *7*, eabg4336. https://doi.org/10.1126/sciadv.abg4336.
6. Song, W., Cheng, D., Hong, S., Sappe, B., Hu, Y., Wei, N., Zhu, C., O'Connor, M.B., Pissios, P., and Perrimon, N. (2017). Midgut-Derived Activin Regulates Glucagon-like Action in the Fat Body and Glycemic Control. Cell Metab. *25*, 386–399. https://doi.org/10.1016/j.cmet.2017.01.002.
7. Kotoulas, O.B., Kalamidas, S.A., and Kondomerkos, D.J. (2006). Glycogen autophagy in glucose homeostasis. Pathol. Res. Pract. *202*, 631–638. https://doi.org/10.1016/j.prp.2006.04.001.
8. Zirin, J., Nieuwenhuis, J., and Perrimon, N. (2013). Role of autophagy in glycogen breakdown and its relevance to chloroquine myopathy. PLoS Biol. *11*, e1001708. https://doi.org/10.1371/journal.pbio.1001708.
9. Wanders, R.J.A., Waterham, H.R., and Ferdinandusse, S. (2015). Metabolic Interplay between Peroxisomes and Other Subcellular Organelles Including Mitochondria and the Endoplasmic Reticulum. Front. Cell Dev. Biol. *3*, 83. https://doi.org/10.3389/fcell.2015.00083.
10. Zhang, X., Yang, S., Chen, J., and Su, Z. (2018). Unraveling the Regulation of Hepatic Gluconeogenesis. Front. Endocrinol. *9*, 802. https://doi.org/10.3389/fendo.2018.00802.
11. Baumbach, J., Xu, Y., Hehlert, P., and Kühnlein, R.P. (2014). Galphaq, Ggamma1 and Plc21C control Drosophila body fat storage. J Genet Genomics *41*, 283–292. https://doi.org/10.1016/j.jgg.2014.03.005.
12. Rajan, A., Housden, B.E., Wirtz-Peitz, F., Holderbaum, L., and Perrimon, N. (2017). A Mechanism Coupling Systemic Energy Sensing to Adipokine Secretion. Dev. Cell *43*, 83–98.e6. https://doi.org/10.1016/j.devcel.2017.09.007.
13. Friedman, A., and Perrimon, N. (2006). High-throughput approaches to dissecting MAPK signaling pathways. Methods *40*, 262–271. https://doi.org/10.1016/j.ymeth.2006.05.002.
14. Wortzel, I., and Seger, R. (2011). The ERK Cascade: Distinct Functions within Various Subcellular Organelles. Genes Cancer *2*, 195–209. https://doi.org/10.1177/1947601911407328.
15. Maik-Rachline, G., Hacohen-Lev-Ran, A., and Seger, R. (2019). Nuclear ERK: Mechanism of Translocation, Substrates, and Role in Cancer. Int. J. Mol. Sci. *20*, 1194. https://doi.org/10.3390/ijms20051194.
16. Boeckeler, K., Rosse, C., Howell, M., and Parker, P.J. (2010). Manipulating signal delivery - plasma-membrane ERK activation in aPKC-dependent migration. J. Cell Sci. *123*, 2725–2732. https://doi.org/10.1242/jcs.062299.
17. Kwon, Y., Mehta, S., Clark, M., Walters, G., Zhong, Y., Lee, H.N., Sunahara, R.K., and Zhang, J. (2022). Non-canonical beta-adrenergic activation of ERK at endosomes. Nature *611*, 173–179. https://doi.org/10.1038/s41586-022-05343-3.
18. Wainstein, E., and Seger, R. (2016). The dynamic subcellular localization of ERK: mechanisms of translocation and role in various organelles. Curr. Opin. Cell Biol. *39*, 15–20. https://doi.org/10.1016/j.ceb.2016.01.007.
19. Lee, G., and Park, J.H. (2004). Hemolymph sugar homeostasis and starvation-induced hyperactivity affected by genetic manipulations of the adipokinetic hormone-encoding gene in Drosophila melanogaster. Genetics *167*, 311–323.
20. Chao, Y.H., Robak, L.A., Xia, F., Koenig, M.K., Adesina, A., Bacino, C.A., Scaglia, F., Bellen, H.J., and Wangler, M.F. (2016). Missense variants in the middle domain of DNM1L in cases of infantile encephalopathy alter peroxisomes and mitochondria when assayed in Drosophila. Hum. Mol. Genet. *25*, 1846–1856. https://doi.org/10.1093/hmg/ddw059.
21. Huang, K., Miao, T., Chang, K., Kim, J., Kang, P., Jiang, Q., Simmonds, A.J., Di Cara, F., and Bai, H. (2020). Impaired peroxisomal import in Drosophila oenocytes causes cardiac dysfunction by inducing upd3 as a peroxikine. Nat. Commun. *11*, 2943. https://doi.org/10.1038/s41467-020-16781-w.
22. Lam, S.S., Martell, J.D., Kamer, K.J., Deerinck, T.J., Ellisman, M.H., Mootha, V.K., and Ting, A.Y. (2015). Directed evolution of APEX2 for electron microscopy and proximity labeling. Nat. Methods *12*, 51–54. https://doi.org/10.1038/nmeth.3179.
23. Hung, V., Udeshi, N.D., Lam, S.S., Loh, K.H., Cox, K.J., Pedram, K., Carr, S.A., and Ting, A.Y. (2016). Spatially resolved proteomic mapping in living cells with the engineered peroxidase APEX2. Nat. Protoc. *11*, 456–475. https://doi.org/10.1038/nprot.2016.018.
24. Isabel, G., Martin, J.R., Chidami, S., Veenstra, J.A., and Rosay, P. (2005). AKH-producing neuroendocrine cell ablation decreases trehalose and induces behavioral changes in Drosophila. Am. J. Physiol. Regul. Integr. Comp. Physiol. *288*, R531–R538. https://doi.org/10.1152/ajpregu.00158.2004.
25. Jansen, R.L.M., Santana-Molina, C., van den Noort, M., Devos, D.P., and van der Klei, I.J. (2021). Comparative Genomics of Peroxisome Biogenesis Proteins: Making Sense of the PEX Proteins. Front. Cell Dev. Biol. *9*, 654163. https://doi.org/10.3389/fcell.2021.654163.
26. Pridie, C., Ueda, K., and Simmonds, A.J. (2020). Rosy Beginnings: Studying Peroxisomes in Drosophila. Front. Cell Dev. Biol. *8*, 835. https://doi.org/10.3389/fcell.2020.00835.
27. James, B.P., Bunch, T.A., Krishnamoorthy, S., Perkins, L.A., and Brower, D.L. (2007). Nuclear localization of the ERK MAP kinase mediated by Drosophila alphaPS2betaPS integrin and importin-7. Mol. Biol. Cell *18*, 4190–4199. https://doi.org/10.1091/mbc.E06-07-0659.
28. Levin, L.R., Han, P.L., Hwang, P.M., Feinstein, P.G., Davis, R.L., and Reed, R.R. (1992). The Drosophila learning and memory gene rutabaga encodes a Ca2+/Calmodulin-responsive adenylyl cyclase. Cell *68*, 479–489. https://doi.org/10.1016/0092-8674(92)90185-f.
29. Copf, T. (2014). Developmental shaping of dendritic arbors in Drosophila relies on tightly regulated intra-neuronal activity of protein kinase A (PKA). Dev. Biol. *393*, 282–297. https://doi.org/10.1016/j.ydbio.2014.07.002.
30. Sanyal, S., Consoulas, C., Kuromi, H., Basole, A., Mukai, L., Kidokoro, Y., Krishnan, K.S., and Ramaswami, M. (2005). Analysis of conditional paralytic mutants in Drosophila sarco-endoplasmic reticulum calcium ATPase reveals novel mechanisms for regulating membrane excitability. Genetics *169*, 737–750. https://doi.org/10.1534/genetics.104.031930.
31. Kim, S.H., Lee, Y., Akitake, B., Woodward, O.M., Guggino, W.B., and Montell, C. (2010). Drosophila TRPA1 channel mediates chemical avoidance in gustatory receptor neurons. Proc. Natl. Acad. Sci. USA *107*, 8440–8445. https://doi.org/10.1073/pnas.1001425107.

32. Banerjee, S., Joshi, R., Venkiteswaran, G., Agrawal, N., Srikanth, S., Alam, F., and Hasan, G. (2006). Compensation of inositol 1,4,5-trisphosphate receptor function by altering sarco-endoplasmic reticulum calcium ATPase activity in the Drosophila flight circuit. J. Neurosci. *26*, 8278–8288. https://doi.org/10.1523/JNEUROSCI.1231-06.2006.

33. Rodriguez, P., Bhogal, M.S., and Colyer, J. (2003). Stoichiometric phosphorylation of cardiac ryanodine receptor on serine 2809 by calmodulin-dependent kinase II and protein kinase A. J. Biol. Chem. *278*, 38593–38600. https://doi.org/10.1074/jbc.C301180200.

34. Wolins, N.E., and Donaldson, R.P. (1997). Binding of the peroxisomal targeting sequence SKL is specified by a low-affinity site in castor bean glyoxysomal membranes. A domain next to the SKL binds to a high-affinity site. Plant Physiol. *113*, 943–949. https://doi.org/10.1104/pp.113.3.943.

35. Faust, J.E., Verma, A., Peng, C., and McNew, J.A. (2012). An inventory of peroxisomal proteins and pathways in Drosophila melanogaster. Traffic *13*, 1378–1392. https://doi.org/10.1111/j.1600-0854.2012.01393.x.

36. Zhou, J., Xu, L., Duan, X., Liu, W., Zhao, X., Wang, X., Shang, W., Fang, X., Yang, H., Jia, L., et al. (2019). Large-scale RNAi screen identified Dhpr as a regulator of mitochondrial morphology and tissue homeostasis. Sci. Adv. *5*, eaax0365. https://doi.org/10.1126/sciadv.aax0365.

37. Just, P.A., Charawi, S., Denis, R.G.P., Savall, M., Traore, M., Foretz, M., Bastu, S., Magassa, S., Senni, N., Sohier, P., et al. (2020). Lkb1 suppresses amino acid-driven gluconeogenesis in the liver. Nat. Commun. *11*, 6127. https://doi.org/10.1038/s41467-020-19490-6.

38. Okun, J.G., Rusu, P.M., Chan, A.Y., Wu, Y., Yap, Y.W., Sharkie, T., Schumacher, J., Schmidt, K.V., Roberts-Thomson, K.M., Russell, R.D., et al. (2021). Liver alanine catabolism promotes skeletal muscle atrophy and hyperglycaemia in type 2 diabetes. Nat. Metab. *3*, 394–409. https://doi.org/10.1038/s42255-021-00369-9.

39. Okamoto, H., Kim, J., Aglione, J., Lee, J., Cavino, K., Na, E., Rafique, A., Kim, J.H., Harp, J., Valenzuela, D.M., et al. (2015). Glucagon Receptor Blockade With a Human Antibody Normalizes Blood Glucose in Diabetic Mice and Monkeys. Endocrinology *156*, 2781–2794. https://doi.org/10.1210/en.2015-1011.

40. Conarello, S.L., Jiang, G., Mu, J., Li, Z., Woods, J., Zycband, E., Ronan, J., Liu, F., Roy, R.S., Zhu, L., et al. (2007). Glucagon receptor knockout mice are resistant to diet-induced obesity and streptozotocin-mediated beta cell loss and hyperglycaemia. Diabetologia *50*, 142–150. https://doi.org/10.1007/s00125-006-0481-3.

41. Banks, A.S., McAllister, F.E., Camporez, J.P.G., Zushin, P.J.H., Jurczak, M.J., Laznik-Bogoslavski, D., Shulman, G.I., Gygi, S.P., and Spiegelman, B.M. (2015). An ERK/Cdk5 axis controls the diabetogenic actions of PPARgamma. Nature *517*, 391–395. https://doi.org/10.1038/nature13887.

42. Lu, X.Y., Shi, X.J., Hu, A., Wang, J.Q., Ding, Y., Jiang, W., Sun, M., Zhao, X., Luo, J., Qi, W., and Song, B.L. (2020). Feeding induces cholesterol biosynthesis via the mTORC1-USP20-HMGCR axis. Nature *588*, 479–484. https://doi.org/10.1038/s41586-020-2928-y.

43. Xue, N., Wei, C., Zhang, L., Liu, H., Wang, X., and Wang, L. (2017). The Characteristics of Hepatic Gsalpha-cAMP Axis in HSHF Diet-Fed Obese Insulin Resistance Rats and Genetic Diabetic Mice. Biol. Pharm. Bull. *40*, 774–781. https://doi.org/10.1248/bpb.b16-00749.

44. Okumoto, K., El Shermely, M., Natsui, M., Kosako, H., Natsuyama, R., Marutani, T., and Fujiki, Y. (2020). The peroxisome counteracts oxidative stresses by suppressing catalase import via Pex14 phosphorylation. Elife *9*, e55896. https://doi.org/10.7554/eLife.55896.

45. Hong, S., Song, W., Zushin, P.J.H., Liu, B., Jedrychowski, M.P., Mina, A.I., Deng, Z., Cabarkapa, D., Hall, J.A., Palmer, C.J., et al. (2018). Phosphorylation of Beta-3 adrenergic receptor at serine 247 by ERK MAP kinase drives lipolysis in obese adipocytes. Mol. Metab. *12*, 25–38. https://doi.org/10.1016/j.molmet.2018.03.012.

46. Jiao, P., Feng, B., Li, Y., He, Q., and Xu, H. (2013). Hepatic ERK activity plays a role in energy metabolism. Mol. Cell. Endocrinol. *375*, 157–166. https://doi.org/10.1016/j.mce.2013.05.021.

47. Mooli, R.G.R., Rodriguez, J., Takahashi, S., Solanki, S., Gonzalez, F.J., Ramakrishnan, S.K., and Shah, Y.M. (2021). Hypoxia via ERK Signaling Inhibits Hepatic PPARalpha to Promote Fatty Liver. Cell. Mol. Gastroenterol. Hepatol. *12*, 585–597. https://doi.org/10.1016/j.jcmgh.2021.03.011.

48. Ramakrishnan, S.K., Zhang, H., Takahashi, S., Centofanti, B., Periyasamy, S., Weisz, K., Chen, Z., Uhler, M.D., Rui, L., Gonzalez, F.J., and Shah, Y.M. (2016). HIF2alpha Is an Essential Molecular Brake for Postprandial Hepatic Glucagon Response Independent of Insulin Signaling. Cell Metab. *23*, 505–516. https://doi.org/10.1016/j.cmet.2016.01.004.

49. Li, Y., Zhou, X., Cheng, C., Ding, G., Zhao, P., Tan, K., Chen, L., Perrimon, N., Veenstra, J.A., Zhang, L., and Song, W. (2023). Gut AstA mediates sleep deprivation-induced energy wasting in Drosophila. Cell Discov. *9*, 49. https://doi.org/10.1038/s41421-023-00541-3.

50. Tang, H.W., Hu, Y., Chen, C.L., Xia, B., Zirin, J., Yuan, M., Asara, J.M., Rabinow, L., and Perrimon, N. (2018). The TORC1-Regulated CPA Complex Rewires an RNA Processing Network to Drive Autophagy and Metabolic Reprogramming. Cell Metab. *27*, 1040–1054.e8. https://doi.org/10.1016/j.cmet.2018.02.023.

51. Schneider, C.A., Rasband, W.S., and Eliceiri, K.W. (2012). NIH Image to ImageJ: 25 years of image analysis. Nat. Methods *9*, 671–675. https://doi.org/10.1038/nmeth.2089.

52. Hong, S., Moreno-Navarrete, J.M., Wei, X., Kikukawa, Y., Tzameli, I., Prasad, D., Lee, Y., Asara, J.M., Fernandez-Real, J.M., Maratos-Flier, E., and Pissios, P. (2015). Nicotinamide N-methyltransferase regulates hepatic nutrient metabolism through Sirt1 protein stabilization. Nat. Med. *21*, 887–894. https://doi.org/10.1038/nm.3882.

53. Wiśniewski, J.R., Zougman, A., Nagaraj, N., and Mann, M. (2009). Universal sample preparation method for proteome analysis. Nat. Methods *6*, 359–362. https://doi.org/10.1038/nmeth.1322.

STAR★METHODS

KEY RESOURCES TABLE

REAGENT or RESOURCE	SOURCE	IDENTIFIER
Antibodies		
Mouse Monoclonal anti-phospho-ERK	Sigma-Aldrich	Cat#M8159; RRID:AB_477245
Rabbit Monoclonal anti-ERK	Cell Signaling Technology	Cat#4695S; RRID:AB_390779
Mouse Monoclonal anti-α-tubulin	Sigma-Aldrich	Cat#T5168; RRID:AB_477579
Rabbit Polyclonal anti-H3	Beyotime	Cat#AH433; RRID:AB_2617171
Rabbit Polyclonal anti-HSP60	Cell Signaling Technology	Cat#4869; RRID:AB_2264430
Rabbit Polyclonal anti-dPMP70	This study	N/A
Mouse Monoclonal anti-GFP	ABclonal	Cat#AE012; RRID:AB_2770402
Mouse Monoclonal anti-FLAG	Sigma-Aldrich	Cat#F1804; RRID:AB_262044
Rabbit Polyclonal anti-PMP70	Sigma-Aldrich	Cat#P0497; RRID:AB_477306
HRP-labeled Streptavidin	Beyotime	Cat#A0303
Goat anti-Mouse IgG (H + L) Highly Cross-Adsorbed Secondary Antibody, Alexa Fluor Plus 594	Thermo Fisher Scientific	Cat#A32742; RRID:AB_2762825
Goat anti-Mouse IgG (H + L) Highly Cross-Adsorbed Secondary Antibody, Alexa Fluor™ Plus 488	Thermo Fisher Scientific	Cat#A32723; RRID:AB_2633275
Goat anti-Rabbit IgG (H + L) Highly Cross-Adsorbed Secondary Antibody, Alexa Fluor™ Plus 488	Thermo Fisher Scientific	Cat#A32731; RRID:AB_2633280
Goat anti-Rabbit IgG (H + L) Highly Cross-Adsorbed Secondary Antibody, Alexa Fluor™ Plus 594	Thermo Fisher Scientific	Cat#A32740; RRID:AB_2762824
Goat anti-Rabbit IgG (H + L) Highly Cross-Adsorbed Secondary Antibody, HRP	Thermo Fisher Scientific	Cat#A16110; RRID:AB_2534782
Goat anti-Mouse IgG (H + L) Highly Cross-Adsorbed Secondary Antibody, HRP	Thermo Fisher Scientific	Cat#A16078; RRID:AB_2534751
Bacterial and virus strains		
DH5α Competent *E.coli* Strain	Vazyme	Cat#C502
Biological samples		
Human liver sample	This study	N/A
Human serum sample	This study	N/A
Chemicals, peptides, and recombinant proteins		
Amyloglucosidase	Sigma-Aldrich	Cat#A7420
Puromycin	Sangon	Cat#A610593
Biotin-phenol	Sigma-Aldrich	Cat#SML2135
RIPA Buffer	Sangon	Cat#C500005
Protease and Phosphatase Inhibitor Cocktail	TargetMol	Cat#C0001, Cat#C0002, Cat#C0003
Streptavidin Magnetic Beads	Thermo Fisher Scientific	Cat#88816
Trypan Blue	Sangon	Cat#E607320
DAPI	Thermo Fisher Scientific	Cat#D1306
Schneider's Drosophila Medium	Thermo Fisher Scientific	Cat#21720024
Critical commercial assays		
Trehalose Assay Kit	Megazyme	Cat#K-Gluc
Glucagon ELISA Kit	R&D Systems	Cat#GCG0D
Effectene Transfection Reagent	QIAGEN	Cat#301425

(*Continued on next page*)

Continued

REAGENT or RESOURCE	SOURCE	IDENTIFIER
ClonExpress MultiS One Step Cloning Kit	Vazyme	Cat#C113
Pierce 660-nm protein assay	Thermo Fisher Scientific	Cat#22660
BCA Protein Asaay Kit	Sangon	Cat#C503021
Peroxisome Isolation Kit	Sigma-Aldrich	Cat#PEROX1
Deposited data		
Proteomics raw and analyzed data	This study	iProX: PXD045176
Metabolomics raw and analyzed data	This study	iProX: PXD045172
Experimental models: Cell lines		
D. melanogaster: Cell line S2R+	Laboratory of Norbert Perrimon, Harvard Medical School	N/A
D. melanogaster: Stable AkhR- and GFP. ERK-expressing S2R + cells	This study	N/A
D. melanogaster: Stable AkhR- and GFP. SKL-expressing S2R + cells	This study	N/A
D. melanogaster: Stable AkhR- and Apex2. ERK-expressing S2R + cells	This study	N/A
Experimental models: Organisms/strains		
D. melanogaster: *R4-Gal4*	Our previous study Song et al.[6]	N/A
D. melanogaster: *Lpp-Gal4*	Our previous study Song et al.[6]	N/A
D. melanogaster: *Cg-Gal4*	Our previous study Song et al.[6]	N/A
D. melanogaster: w^{1118}	Our previous study Song et al.[6]	N/A
D. melanogaster: *UAS-w-RNAi*	Our previous study Song et al.[6]	N/A
D. melanogaster: Akh^{A}	Our previous study Li et al.[49]	N/A
D. melanogaster: *UAS-Akh*	Bloomington Stock Center	BDSC_27343
D. melanogaster: *UAS-ERK-i-v*	Vienna Drosophila Resource Center	V109108
D. melanogaster: *UAS-ERK-i-h*	Bloomington Stock Center	BDSC_34855
D. melanogaster: *UAS-AkhR-i*	Bloomington Stock Center	BDSC_29577
D. melanogaster: *UAS-msk-L*	Bloomington Stock Center	BDSC_23944
D. melanogaster: *UAS-Pka.C1*	Bloomington Stock Center	BDSC_35555
D. melanogaster: *UAS-rut*	Bloomington Stock Center	BDSC_9405
D. melanogaster: *UAS-SERCA-i*	Bloomington Stock Center	BDSC_25928
D. melanogaster: *UAS-TrpA1*	Bloomington Stock Center	BDSC_26263
D. melanogaster: *UAS-Itpr-i*	TsingHua Fly Center	THU2114
D. melanogaster: *UAS-CaMKII-i*	Bloomington Stock Center	BDSC_29401
D. melanogaster: *UAS-InR-i*	Bloomington Stock Center	BDSC_31037
D. melanogaster: $UAS\text{-}InR^{AC}$	Bloomington Stock Center	BDSC_8248
D. melanogaster: *UAS-Pex1-i1*	TsingHua Fly Center	THU0496
D. melanogaster: *UAS-Pex1-i2*	TsingHua Fly Center	TH01857.N
D. melanogaster: *UAS-Pex5-i*	TsingHua Fly Center	TH02247.N
D. melanogaster: *UAS-Pex7-i1*	TsingHua Fly Center	TH01894.N
D. melanogaster: *UAS-Pex7-i2*	TsingHua Fly Center	TH201500691.S
D. melanogaster: *UAS-Pex13-i1*	TsingHua Fly Center	TH01887.N
D. melanogaster: *UAS-Pex13-i2*	TsingHua Fly Center	TH201500684.S
D. melanogaster: *UAS-Pex14-i1*	TsingHua Fly Center	TH01902.N
D. melanogaster: *UAS-Pex14-i2*	TsingHua Fly Center	TH201500685.S
D. melanogaster: *UAS-mCD8.mRFP.LG*	Bloomington Stock Center	BDSC_27399
D. melanogaster: *UAS-mCherry.mito.OMM*	Bloomington Stock Center	BDSC_66533
D. melanogaster: *UASp-RFP.Golgi*	Bloomington Stock Center	BDSC_30908
D. melanogaster: *UASp-RFP.KDEL*	Bloomington Stock Center	BDSC_30910

(*Continued on next page*)

Continued

REAGENT or RESOURCE	SOURCE	IDENTIFIER
D. melanogaster: *UAS-Atg8a.m.Cherry*	The previous study Tang at al.[50]	N/A
D. melanogaster: *UAS-GFP.SKL*	Bloomington Stock Center	BDSC_28881
D. melanogaster: *UAS-GFP.SKL*	Bloomington Stock Center	BDSC_28882
D. melanogaster: *UAS-Rab11-GFP*	Bloomington Stock Center	BDSC_8506
D. melanogaster: *UAS-GFP-LAMP1*	Bloomington Stock Center	BDSC_42714
Oligonucleotides		
Primer for cloning of *AkhR*, forward: CCTACTAGTCCAGTGTGGTGGAATT CATGGCAAAAGTAGCTGAGGA	This study	N/A
Primer for cloning of *AkhR*, reverse: AGTAGGCTGCCGCGTCCTTCGCGG CCGCCCTTCTGGCGGATCGGGGA	This study	N/A
Primer for cloning of *ERK*, forward: GGCATGGACGAGCTGTACAAGCTT ATGGAGGAATTTAATTCGAGCG	This study	N/A
Primer for cloning of *ERK*, reverse: TAGAAGACTTCCTCTGCCCTCAAG CTTAGGCGCATTGTCTGGTTGTC	This study	N/A
Primer for cloning of *GFP.SKL*, forward: GATATCTCTAGAGCCACCATGGTGAG CAAGGGCGA	This study	N/A
Primer for cloning of *GFP.SKL*, reverse: CTGCCCTCAAGCTTATGTTTGCTGTA CAGCTCGTCCATG	This study	N/A
Recombinant DNA		
pAc5-stable2-puro	Our previous study Song et al.[6]	N/A
pAc5-AkhR-T2A-GFP.ERK-T2A-Puro	This study	N/A
pAc5-AkhR-T2A-GFP.SKL-T2A-Puro	This study	N/A
pAc5-AkhR-T2A-FLAG.APEX2.ERK-T2A-Puro	This study	N/A
Software and algorithms		
Prism 8	GraphPad	http://www.graphpad.com/scientificsoftware/prism/
ImageJ	Schneider et al.[51]	https://imagej.nih.gov/ij/
Adobe Photoshop CS6	Adobe	https://www.adobe.com
R (v4.0.3)	R Core Team	https://www.r-project.org
LAS X	Leica	https://www.leica-microsystems.com
ZEN	Zeiss	https://www.zeiss.com

RESOURCE AVAILABILITY

Lead contact

Further information and requests for resources and reagents should be directed to and will be fulfilled by the Lead Contact, Wei Song(songw@whu.edu.cn).

Materials availability

All stable reagents generated in this study are available from the lead contact without restriction.

Data and code availability

Raw and analyzed data for APEX2-ERK-associated proteomics and Akh-associated metabolomics are publicly available at iProX: PXD045176 and iProX: PXD045172, respectively. This paper does not report original code. Any additional information required to reanalyze the data reported in this paper is available from the lead contact upon request.

EXPERIMENTAL MODEL AND STUDY PARTICIPANTS DETAILS

Fly strains and rearing

Files were raised on fly food (5 g agar, 25 g dry yeast, 75 g corn flour, 90 g sucrose, 1.25 g Methylparaben, 4 mL propionic acid per liter) in incubator 12 h light/12 h dark cycle at 25°C. For high-sugar feeding, eggs were laid and then larvae were cultured on high-sugar food (25% extra sucrose was added into our fly food) through development. All the experiments were performed at late 3rd instar stage (12∼24h before wandering). Late 3rd instar larvae were cultured in starvation food (1% agar only) for 4 h to evaluate Akh response. Genotype of *AKH*-overexpressing flies is *UAS-Akh; R4-Gal4/T(2;3)B3, CyO: TM6B, Tb.* Negative controls, w^{1118} and *UAS-w-RNAi,* exhibited similar phenotypes and only w^{1118} is shown in the figures.

Mouse models

All mouse work was approved by the Animal Care and Ethical Committee at Wuhan University. *C57BL/6* male mice (6–8 weeks old) weighing 18–22 g were purchased from GemPharmatech, China. Mice were kept under an automated 12 h light/dark cycle at a controlled relative humidity of 40–50%, temperature of 22 ± 2°C and had *ad libitum* access to a standard dry diet and tap water. The high-fat high-sucrose diet (HFHS, Research Diets, D12468) was used to develop diet-induced obesity. Sample size, determined empirically via performing preliminary experiments, was chosen to ensure that adequate statistical power was achieved.

For glucagon tolerance test, 8-week-old male mice were intraperitoneally (IP) injected with Vehicle or Trametinib (3 mg/kg/day) for 5 days. Mice were IP administered with glucagon (100 μg/kg). Glucose levels in the blood from venous were measured at different time points using a glucometer (Yuwell).

Human samples

Surgical liver samples were collected from obese patients (BMI>25) with (14 patients) or without (19 patients) diabetes (Oral Glucose Tolerance Test 2h > 11.1 and or Fasting Plasma Glucose >7.0) at Department of Hepatobiliary and Pancreatic Surgery, Zhongnan Hospital of Wuhan University between January 2018 and January 2019 (the detail information of these patients was listed in the table as below). Surgical samples were taken on the day of laparoscopic sleeve gastrectomy (LSG) or laparoscopic Roux-en-Y gastric bypass (LRYGB). Blood samples were obtained after overnight fasting. Serum from blood samples was collected after centrifugation at 1,000 *g* for 15 min at room temperature. 50 μL serum was 1:4 diluted with 150 μL dilution buffer to measure glucagon concentration using commercial ELISA kits (DGCG0, R&D Systems).

Written informed consents were obtained from all participants in this study. This study protocol conformed to the ethical guidelines of the 1975 Declaration of Helsinki principles and was approved by the Human Ethics Committee of Zhongnan Hospital of Wuhan University.

Primary hepatocyte isolation and culture

Primary hepatocytes were isolated from male 8-12-week-old mice as described previously.[52] Briefly, the mouse abdominal cavity was opened after anesthesia. A needle was used to puncture the portal vein with 50 mL wash buffer (Krebs Ringer buffer containing 3.6 mg/mL glucose, 0.1 mM EGTA) and 50 mL collagenase perfusion (Krebs Ringer buffer containing 3.6 mg/mL glucose, 1.372 mM $CaCl_2$, 0.04% Collagenase Type I (Worthington) at 37 °C. When liver was digested completely, it was excised and washed in ice-cold Dulbecco's Modified Eagle's Medium (DMEM) for 3 times. Then the liver was minced and filtered through a 70-μm cell strainer (Fisher) into a 50-mL centrifuge tube. Cells were then washed with cold DMEM for three times and re-suspended in 15 mL of cold DMEM supplemented with 10% FBS, 2 mM L-glutamine, 20 units/mL penicillin and 20 μg/mL streptomycin. After the viability was determined by Trypan Blue staining, hepatocytes were seeded on collagen-coated plates at a density of 400,000/mL for at least 8 h prior to further assays.

METHOD DETAILS

Carbohydrate measurements in 3rd instar larvae

The method of circulating trehalose measurement was previously described.[6] Briefly, 2 μL hemolymph from 3rd instar larvae was diluted in 58 μL sugar buffer (5 mM Tris [pH 6.6], 137 mM NaCl, 2.7 mM KCl) and heated at 70°C for 5 min to inactivate endogenous trehalase. For high sugar diet larvae or *Akh* overexpression larvae, we diluted 1 μL hemolymph to 59 μL PBS. After brief centrifugation of 1,000 *g* for 10 min at 4°C, 10 μL supernatant was treated with 0.2 μL water or trehalase (Megazyme, E-TREH) at 37°C for 20 min to digest trehalose into glucose, and glucose was measured by incubation with 150 μL glucose assay reagent (Megazyme, K-GLUC) at 37°C for 5 min. The absorbance at 510 nm was measured on a SpectraMax Paradigm plate reader. The circulating trehalose levels were determined by subtracting the circulating free glucose levels from the total glucose levels after enzyme digestion. We defined circulating trehalose as glycemic level in this study.

The measurement of carbohydrate stored in larval fat body has been previously described.[6] 10 3rd instar larval fat bodies were homogenized in 500 μL PBS containing 0.2% Triton X- and protease inhibitor and heated at 70°C for 5 min to inactivate endogenous enzymes. After centrifugation at 13,000 rpm for 10 min at 4°C, 10 μL supernatant of lysate was treated with 0.8 μL Amyloglucosidase (Sigma, A7420, for glycogen measurement) at 37°C for 20 min, and glucose level was measured using glucose assay reagent

(Megazyme, K-GLUC). 10 μL supernatant was used for protein level measurement using BCA reagent (Sangon, C503021). The final glycogen amount was determined by subtracting free glucose levels from total glucose levels after enzyme digestion and then normalized to protein levels.

Generation of stable AkhR- and Apex2.ERK-expressing S2R + cells

Full-length cDNAs of AkhR and fusion protein FLAG.Apex2.ERK were cloned by RT-PCR using primers as below.

Gene	Primer
AkhR-F	CCTACTAGTCCAGTGTGGTGGAATTCATGGCAAAAGTAGCTGAGGA
AkhR-R	AGTAGGCTGCCGCGTCCTTCGCGGCCGCCCTTCTGGCGGATCGGGGA
FLAG.APEX2-F	CCTGGCCCTGGTTCCGATATCGATTACAAGGACGACGATGACAAGGGAAAGTCTTACCC
FLAG.APEX2-R	AATTAAATTCCTCCATGGCATCAGCAAACCCAAGC
ERK-F	GCTTGGGTTTGCTGATGCCATGGAGGAATTTAATTCGAGCG
ERK-R	TAGAAGACTTCCTCTGCCCTCAAGCTTAGGCGCATTGTCTGGTTGTC

The fragments were assembled into the plasmid vector pAC5.1-Stable2-Puro[6] using ClonExpress Ultra One Step Cloning Kit (Vazyme, C113) to generate pAC5-AkhR-T2A-FLAG.APEX2.ERK-T2A-Puro, which allows for multicistronic expression of the target proteins as well as a protein conferring puromycin resistance. S2R + cell transfection was performed using the non-liposomal reagent Effectene (Qiagen) following the manufacturer's instructions. 60 h after transfection, cells were incubated for two weeks in selective medium, Schneider's medium (Thermo) containing 10% FBS, standard cell culture antibiotics, and 10 μg/mL puromycin. Cells were split as necessary and again incubated in selective medium. Stable cells were maintained with selective medium and AKH treatment performed in medium without puromycin.

APEX2 reaction and biotinylated protein capture

After treatment of Schneider's Medium without FBS for 30 min, AkhR-plus-Apex2.ERK-expressing S2R + cells were incubated with or without 10 nM AKH and 2.5 mM biotin-phenol (BP) for 30 min, then treated with 1 mM H_2O_2 for 1 min to initiate biotinylation. The medium was immediately discarded. Following softly wash with quencher solution for four times, cells were lysed with RIPA buffer (Sangon Biotech, C500005) with protease and phosphatase inhibitor cocktail (TargetMol, C0001, C0002, C0003) on ice for 5–10 min. After centrifugation of 15,000 *g* for 10 min at 4°C, the supernatant was collected for protein quantification using Pierce 660-nm protein assay regent (Thermo Scientific, 22660). Cell lysate containing ~360 μg protein was incubated with 30 μL streptavidin magnetic beads for 2h at RT on a rotator. After washing with wash buffers to remove nonspecific binders on a magnetic rack on ice, beads were further boiled with 30 μL elution buffer (3X protein loading buffer containing with 2 mM biotin and 20 mM DTT) to eluted biotinylated proteins for further proteomic analysis.

Proteomics and data analysis

Label-free quantitative proteomics was performed by Bioprofile Biotech Ltd. Protein (200 μg for each sample) digestion was performed with FASP method described by Wisniewski, Zougman et al.[53] Briefly, the detergent, DTT and IAA in UA buffer was added to block reduced cysteine. Finally, the protein suspension was digested with trypsin (Promega) at ratio 50:1 overnight at 37°C. The peptides were collected by centrifugation at 16,000 *g* for 15 min. The peptide was desalted with C18 StageTip for further LC-MS/MS analysis.

LC-MS/MS were performed on a Q Exactive Plus mass spectrometer coupled with Easy-nLC 1200 (Thermo Fisher Scientific). Peptides were loaded on to a Trap Column (100 μm × 20 mm, 5 μm, C18, Dr. Maisch GmbH, Ammerbuch, Germany) in buffer A (0.1% formic acid in water), then were injected and separated by a chromatographic column (75 μm × 150 mm; 3 μm, C18, Dr. Maisch GmbH) at a flow rate of 300 nL/min. The liquid phase separation gradient is as follows: 0–2 min, 5–8%, B (0.1% formic acid in 95% acetonitrile); 2–90 min, 8–23%, B; 90–100 min, 23–40%, B; 100–108 min, 40–100%, B; 108–120 min, buffer B maintained at 100%. DDA (Data Dependent Acquisition) mass spectrometric analysis using a Q-Exactive HF-X mass spectrometer (Thermo Scientific) after peptide separation. The analysis time was 120 min, detection model: positive ion, parent ion scanning range: 300–1800 m/z, primary mass spectrometric resolution: 60,000 m/z 200. Secondary mass spectrogram of 20 parent ions with the highest intensity was acquired after each full scan, resolution: 15,000 m/z 200.

The LC-MS/MS RAW data were imported into the search engine Sequest HT in the Proteome Discoverer software (version 2.4, Thermo Scientific). The database we used in this experiment is Uniprot-*Dorsophila Melanogaster* (https://www.uniprot.org/taxonomy/). The quantitative protein ratios were weighted and normalized by the median ratio in Maxquant software. Only proteins with fold change >1.25-fold were considered for significantly differential expressions.

Metabolomics and data analysis

The metabolomics analysis was performed by Bioprofile Biotech, Ltd. 100 μL larval hemolymph was thoroughly mixed with 400 μL of cold methanol acetonitrile (v/v, 1:1) via vortex. And then the mixture was processed with sonication for 1 h in ice baths. The mixture was then incubated at −20°C for 1 h, and centrifuged at 4°C for 20 min with a speed of 14,000 *g*. The supernatants were then harvested and dried under vacuum for LC-MS analysis. Metabolomics profiling was analyzed using a UPLC-ESI-Q-Orbitrap-MS system (UHPLC, Shimadzu Nexera X2 LC-30AD, Shimadzu, Japan) coupled with Q-Exactive Plus (Thermo Scientific, San Jose, USA). Quality control (QC) samples were prepared by pooling aliquots of all samples that were representative of the samples under analysis, and used for data normalization. The raw MS data were processed using MS-DIAL for peak alignment, retention time correction and peak area extraction. The metabolites were identified by accuracy mass (mass tolerance <0.01Da) and MS/MS data (mass tolerance <0.02Da) which were matched with HMDB, MassBank and other public databases and our self-built metabolite standard library. In the extracted-ion features, only the variables having more than 50% of the nonzero measurement values in at least one group were kept.

R (version:4.0.3) and packages were used for all multivariate data analyses and modeling. Data were mean-centered using Pareto scaling. Models were built on principal component analysis (PCA), orthogonal partial least-square discriminant analysis (PLS-DA) and partial least-square discriminant analysis (OPLS-DA). All the models evaluated were tested for over fitting with methods of permutation tests. OPLS-DA allowed the determination of discriminating metabolites using the variable importance on projection (VIP). Metabolites with VIP >1.0 and $p < 0.05$ were considered as statistically significant changed. To identify the perturbed biological pathways, the differential metabolite data were performed KEGG pathway analysis using KEGG database (http://www.kegg.jp).

Hepatocyte glucose production

Primary mouse hepatocytes were plated on collagen I-coated 24-well plates. Hepatocytes were starved for 3 h and washed twice with PBS. Following this, hepatocytes were incubated in glucose-free DMEM (Sigma) supplemented with 1 mM sodium pyruvate, 2 mM L-glutamine, and 15 mM HEPES, without phenol red. After treatment of 1 μM glucagon with or without 100 nM Trametinib for 4 h, 100 μL medium was collected for glucose quantification using glucose reagent (Megazyme, K-GLUC). The cells were lysed in 80 μL RIPA buffer (Sangon Biotech, C500005) on ice for 15 min and centrifuged at 12,000 rpm for 10 min for protein quantification using BCA regent (Sangon, C503021). We subtracted the amount of free glucose from non-treat hepatocytes and normalized the subtracted values to protein levels in the supernatant.

Organelle isolation and Western blotting

For nuclear isolation, 3rd instar larval fat bodies or S2R + cells were homogenized in 450 μL Buffer I (10 mM HEPES, 1.5 mM $MgCl_2$, 10 mM KCl, 25 mM NaF, 1 mM Na_3VO_4, pH 8.0) containing protease and phosphatase inhibitor Cocktail (TargetMol, C0001, C0002, C0003) using KIMBLE Dounce tissue grinder set (Sigma, D8938) in a 2 mL Dounce homogenizer tube on ice. After incubation on ice for 15 min, 50 μL NP-40 was added to the lysate for a 10-s vortex. Centrifuge tube at 15,000 rpm for 2–3 min at 4°C, transfer the supernatant to a fresh tube. This fraction was the cytoplasmic fraction. Collect the pellet in 220 μL Buffer II (20 mM HEPES, 1.5 mM $MgCl_2$, 450 mM NaCl, 0.2 mM EDTA, 25% glycerol, 25 mM NaF, pH 8.0) containing protease and phosphatase inhibitor Cocktails (TargetMol, C0001, C0002, C000). Shake gently for 30 min at 4°C, centrifuge tube at 15000 rpm for 15 min at 4°C. Transfer the supernatant to a clean, chilled tube. This fraction was the nuclear fraction.

Peroxisomes were extracted from cells using a fractionation centrifugation method. The series of centrifugations were adjusted from the protocol provided by Sigma-Aldrich (Peroxisome Isolation kit, PEROX1, Sigma-Aldrich, St. Louis, MO, USA). Briefly, S2R + cells were incubation with FBS-free Schneider's Medium for 30 min and treated with or without 10 nM Akh for 30 min. Cells were harvested and added in peroxisome extraction buffer. Cells were homogenized using Pestle B in a 7 mL Dounce homogenizer tube to achieve 80–85% breakage on ice. Centrifuge tube at 1,000 *g* for 10 min at 4°C. The supernatant was transferred to a new centrifuge tube and centrifuge at 2,000 *g* for 10 min at 4°C. Transfer the supernatant and centrifuge at 25,000 *g* for 20 min. Remove the supernatant liquid and collect the pellet in a peroxisome extraction buffer. That was the crude peroxisomal fraction (CPF). The CPF was used to prepare the solution according to the protocol. Centrifuge ultracentrifuge tube at 100,000 *g* for 1.5 h in 4°C. Then we can collect individual components and get purified peroxisomes.

S2R + cells and 3rd instar larval fat bodies were lysed in RIPA buffer (Sangon Biotech, C500005) containing protease and phosphatase inhibitor cocktails (TargetMol, C0001, C0002, C0003). Extracts or solutions containing isolated organelles were immunoblotted with Streptavidin (1:2000, Beyotime, A0303) or indicated primary antibodies: mouse anti-phospho-ERK (pERK) (1:2000, Sigma, M8159), rabbit anti-ERK (1:2000, Cell Signaling, 4695S), mouse anti-α-tubulin (1:5000, Sigma, T5168), rabbit anti-H3 (1:1000, Beyotime, AH433), rabbit anti-Hsp60 (1:2000, Cell Signaling, 4869), rabbit anti-dPMP70 (1:2000, this study), mouse anti-GFP (1:2000, ABclonal, AE012), mouse anti-FLAG (1:2000, Sigma, F1804).

Generation of rabbit polyclonal anti-PMP70 antibodies

Polyclonal antibodies *Drosophila* PMP70 were prepared by Mabnus Biotech in Wuhan, China. The synthetic peptides, *Drosophila* PMP70 C-terminal region 646–665 (DGRGSYEFATIDQDKDHFGS), were used for immunizing rabbits for four times. The affinity column was made by coupling 5 mg purified PMP70 peptide to CNBr-activated Sepharose 4B from GE. The antiserum was applied onto the column, the specific antibody was eluted with the Glycine HCl buffer at pH 2.5, followed by dialysis and concentration.

Immunostaining and immunohistochemistry

Larval fat bodies and S2R + cells were fixed for 15 min in PBS containing 4% paraformaldehyde. After fixation, the samples were washed with PBST (0.2% Triton X-100 in PBS) and blocked with 1% BSA in PBST. After incubation with primary antibodies PMP70 (1:500, this study) or pERK (1:100, Sigma, M8159) overnight at 4°C, the tissues were washed and then incubated with Alexa fluorescence secondary antibody (1:1000, Thermo Fisher) and DAPI (1:1000, D1306, Thermo Fisher) for 1 h at room temperature then washed.

Larval fat bodies, mouse and human liver samples were fixed in PBS containing 4% paraformaldehyde, and cryosections or paraffin sections were performed following standard protocols by Servicebio at Wuhan, China. After incubation with primary antibodies like PMP70 (1:500, Sigma, P0497) or pERK (1:500, Sigma, M8159) overnight at 4°C, the tissues were washed and then incubated with Alexa fluorescence secondary antibody (1:1000, Thermo Fisher) and DAPI (1:1000, D1306, Thermo Fisher) or HRP secondary antibody (1:200, Servicebio, G1214) for 1 h at room temperature then washed. Confocal images were obtained using the Zeiss LSM880, Leica STELLARIS 5, and 3DHISTECH Pannoramic MIDI-II.

QUALIFICATION AND STATISTICAL ANALYSIS

Data are presented as the mean ± SEM. Unpaired Student's t test and one-way ANOVA followed by post-hoc test were performed to assess differences. A p value of <0.05 was considered statistically significant.